



A review of vision-aided robotic welding

Ting Lei ^{a,b}, Youmin Rong ^{a,b}, Hui Wang ^{a,b}, Yu Huang ^{a,b,*}, Min Li ^c



^a School of Mechanical Science and Engineering, Huazhong University of Science and Technology, Wuhan, China

^b State Key Lab of Digital Manufacturing Equipment and Technology, Huazhong University of Science and Technology, Wuhan, China

^c Key Lab of Optoelectronic Chemical Materials and Devices (Jianghan University), Ministry of Education, China

ARTICLE INFO

Article history:

Received 13 June 2020

Received in revised form 3 August 2020

Accepted 22 September 2020

Available online 26 October 2020

Keywords:

Robotic welding

Computer vision

Vision sensing

Image processing

Seam tracking

ABSTRACT

Vision-aided robotic welding has been applied in the industrial field for decades. This paper summarizes the procedures of vision-aided robotic welding. Various methods in vision sensor calibration and hand-eye calibration have been illustrated. The recognition, calculation and guidance control are the basic stages of visual positioning for SWP (start welding point). Various groove types (I-groove, V-groove, Y-groove, U-groove etc.) and joint types (butt joint, lap joint, fillet joint, T-joint etc.) can be detected by six active vision sensing methods and three passive vision sensing methods. Weld path detection, tracking algorithm and control strategy are the necessary procedures to realize seam tracking. Various seam trajectories (straight line, zig-zag, sine, half-moon, pipe curve, spatial curve etc.) can be compensated by several common control methods (PID control, fuzzy control, iterative learning control, trajectory-based control etc.). The selection of control method is determined by weld path detection and seam tracking algorithm. In the end, the future development of vision-aided robotic welding has also been presented.

© 2020 Elsevier B.V. All rights reserved.

Contents

1.	Introduction	2
1.1.	The importance of this topic	2
1.2.	The main development	2
1.3.	The overall layout of the paper	4
2.	Pre-weld calibration	4
2.1.	Vision sensor calibration	4
2.1.1.	Camera model	4
2.1.2.	Camera calibration	5
2.2.	Hand-eye calibration	6
3.	The positioning of SWP	10
3.1.	Teach-playback	10
3.2.	Visual guidance	10
3.2.1.	The recognition of SWP	10
3.2.2.	Calculating the coordinates of SWP	11
3.2.3.	Guiding control of SWP	12
4.	Vision sensing	13
4.1.	Active vision sensing	13
4.1.1.	Single-line laser	13
4.1.2.	Cross-lines laser	14
4.1.3.	Multi-lines laser	14
4.1.4.	Grid-lines laser	15

* Corresponding author at: School of Mechanical Science and Engineering, Huazhong University of Science and Technology, Wuhan, China.

E-mail addresses: leiting0621@hust.edu.cn (T. Lei), yuhuang7208@163.com (Y. Huang).

4.1.5.	Dot matrix laser	15
4.1.6.	Circular laser.....	16
4.2.	Passive vision sensing	17
4.2.1.	Welding layer measurement.....	17
4.2.2.	Weld pool detection.....	18
4.2.3.	Swing arc extraction.....	19
5.	Compensation and control	19
5.1.	Weld path detection.....	19
5.1.1.	Front distance detection.....	19
5.1.2.	Current position detection	22
5.1.3.	The generation of weld path	22
5.2.	Seam tracking algorithm	22
5.3.	Robot control strategy.....	25
6.	Review process.....	25
7.	Conclusions and future development	27
7.1.	Conclusions.....	27
7.2.	The future development	27
	Funding	27
	Availability of data and material	27
	Code availability	27
	Authors' contributions	27
	References	27

1. Introduction

1.1. The importance of this topic

Robotic welding has been widely used in ship building (Lee, 2014), pressure vessel processing (Jin et al., 2017), automobile producing (Liu et al., 2010), aircraft parts joining (Zhang et al., 2015a) and railway carriages manufacturing (Kochan, 2000) etc. The welding quality and working efficiency of robotic welding have a significant impact on the industrial field. Ku et al. (2010) developed a self-driving mobile welding robot to weld the U-shaped welding areas in the enclosed double-hull structures. Humans can be replaced by the robot to pass through an access hole 600 mm wide and 800 mm high. Le et al. (2018) adopted a wheeled mobile robot to track the rectangular fillet weld in the shipyard and the steel structure workshop. Humans can avoid working in such a harsh environment. Lü et al. (2017) presented an improved sliding mode control seam tracking method with a low-pass filter for mobile robot to locate the weld line. This can improve working efficiency.

The welding robots are superior to technical workers, focusing in the following aspects: maintaining the consistency of welding quality (Rout et al., 2019), keeping continuous and repetitive work (Li et al., 2017), ensuring accurately weld seam tracking (Wei et al., 2011) etc. However, simple robotic welding has become increasingly unsuitable for modern production. This is because the welding process is inherently nonlinear, multivariable-coupled and uncertain. The robots can't adapt to the complicated situations as accurately and quickly as humans. Simple robotic welding is difficult to achieve precise control (Chen et al., 2010). Nowadays, the application of vision sensor in robotic welding has become an attractive research field (Chen et al., 2005). At present, vision-aided robotic welding mainly has the following functions.

Vision sensor can provide human-like eyes for welding robot, which can confirm the position of SWP. Chen et al. (2013) proposed a visual control method of welding robot to recognize SWP for the thin steel plate butt welding of containers. Zhu et al. (2005) recognized the initial position of weld seam based on the image pattern match technology. (Fan et al. (2019a) designed an active vision sensing system to obtain the 3D (three dimension) coordinates of initial weld point.

Vision sensing can realize welding characteristics monitoring and weld seam tracking. De et al. (De and Parle, 2003) extracted the geometrical parameters of the welding arc using a simple CCD (charge coupled device) monochrome camera. Gao et al. (2011) presented a weld-pool image centroid algorithm to detect the offset between the arc and the seam centerline. Kiddee et al. (2016) utilized a camera with cross mark structured light and a modified matching template to detect the edges of V-groove.

The visual technology has become a practical tool for robot to sense the external environment. There are a lot of academic researches and engineering development on vision-aided robotic welding. They mainly focus on calibration, sensing, algorithm and control, etc. The procedures of vision-aided robotic welding can be divided into pre-weld calibration (Zou and Chen, 2018), autonomous positioning SWP (Chen and Chen, 2010), vision sensing (Zhang et al., 2015b), compensation (Xu et al., 2015) and control (Chen and Lv, 2014). As shown in Fig. 1. These technologies promote the efficiency, operability and quality of robotic welding. Therefore, this topic is essential to review.

1.2. The main development

Robotic welding has evolved from automatic welding special equipment, teach-playback robots to robots with human-like eyes (vision-aided robot). In the future, it will develop into intelligent robots with the ability of independent thinking and self-learning. As shown in Fig. 2. The automatic welding special equipment can reduce manual operation and improve welding efficiency. However, only specific weldment can be welded. Teach-playback robots are utilized in many small and medium-size factories. They are programmed for various weld trajectories. Ma et al. (2010) manipulated a teach-playback welding robot to weld the thin plate closed-gap butts weld. The positioning of SWP can also be realized by the teach-playback robots (Chen et al., 2006). However, the manipulation of the teach-playback robots depends on the experience of the operators. Meanwhile, the motion of welding torch cannot be self-rectified to fit the state of the weldment.

The Robots with human-like eyes, namely vision-aided robot, can not only realize the automatic positioning of SWP, but also realize the welding monitoring and weld seam tracking. The welding

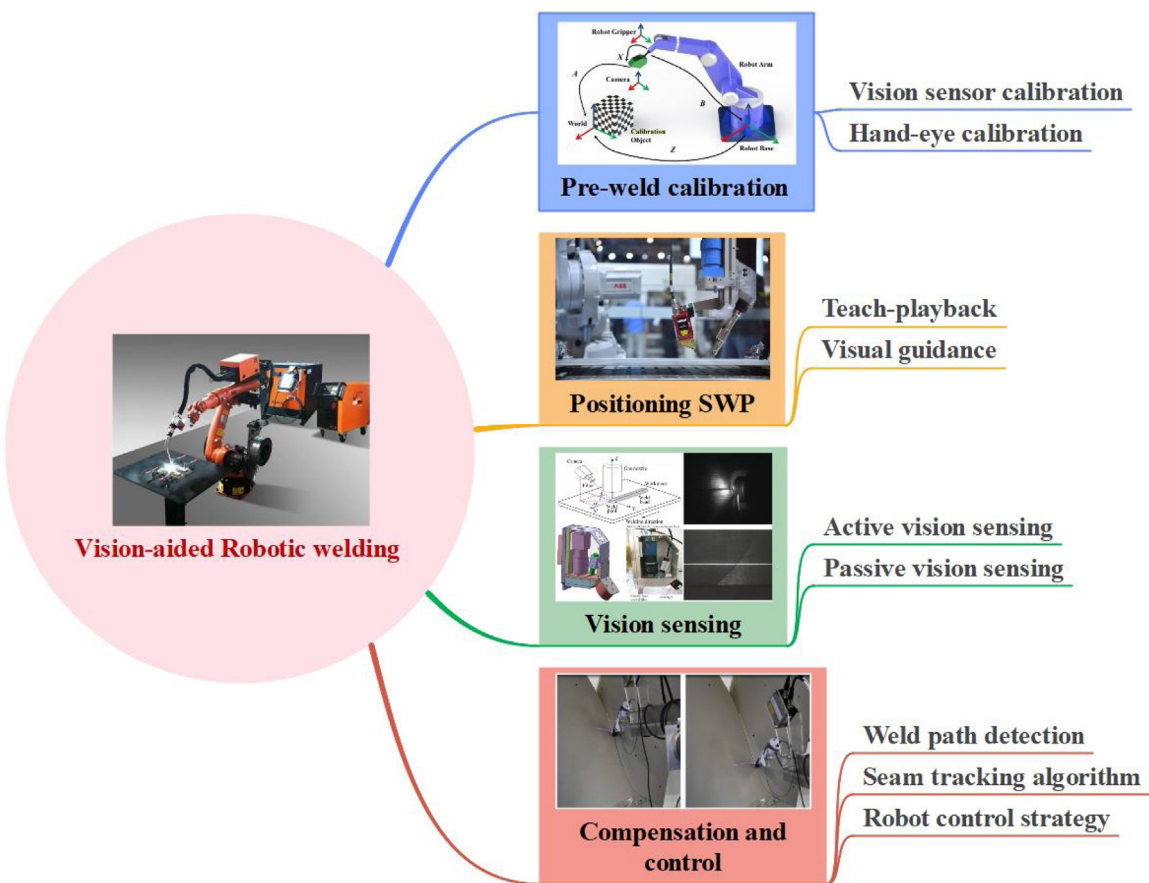


Fig. 1. The procedures of vision-aided robotic welding.

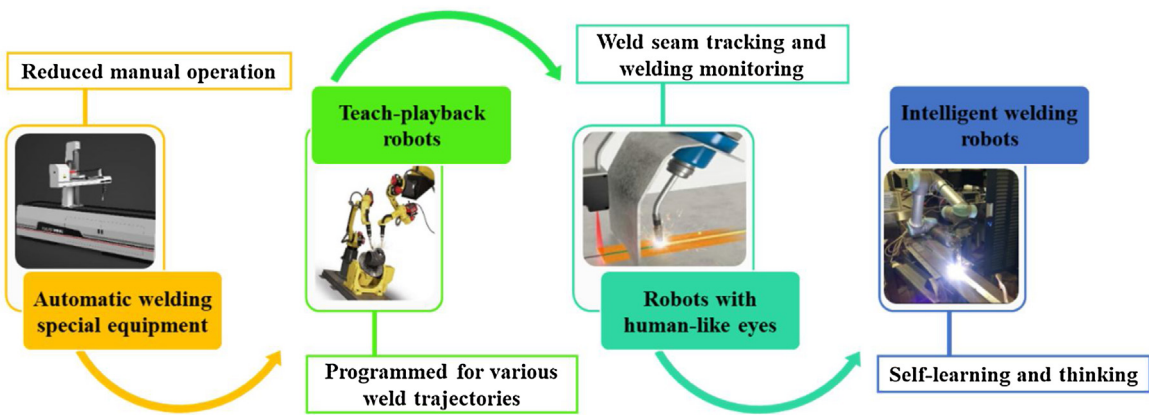


Fig. 2. The development of robotic welding.

layer (Xiong and Zhang, 2013), weld pool (Xu et al., 2012) and swing arc (Li et al., 2015a) can be monitored by vision sensing. This is contributed to understand the welding state and control the welding quality. Shah et al. (2017) detected and recognized the straight line, zig-zag and half-moon line from an active vision sensing system. Li et al. (2008) presented a binocular stereo vision tracking system. The 3D coordinates of the contact head on planar target can be directly computed. Several researchers have proposed some tracking algorithms successfully, such as particle swarm algorithm (Liu et al., 2014), Kalman filtering algorithm (Chen et al., 2011), adaptive feature extraction algorithm (Xiao et al., 2019) and modified Hough algorithm (Wu et al., 2015) etc.

The concept of intelligent welding robots is a recent development. The abilities of self-learning and self-thinking are the typical characteristics of intelligent welding robots. At present, there are also some researches on intelligent control methods (Lai et al., 2018), i.e., neural networks, self-learning strategies and machine learning (Pablo and Manuel, 2019) etc. Wang et al. (2019) trained a HMM (hidden Markov model) by collecting and utilizing the human hand movement speed in the actual welding operation. The human IR (intention recognition) algorithm can be established. The robot can assist the operators to finish a better performance welding task with IR. Although the welding effect is good, there is still a long distance for successful application in industrial production.

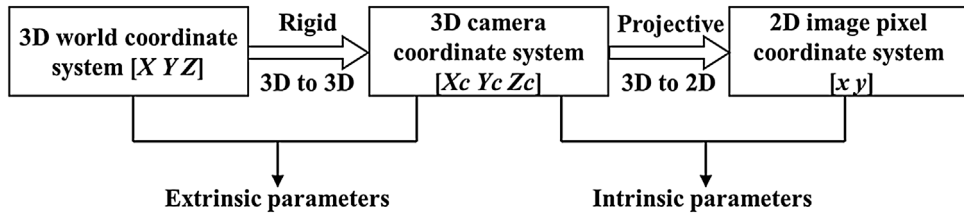


Fig. 3. The coordinate transformation of intrinsic and extrinsic parameters.

1.3. The overall layout of the paper

This paper can be divided into 6 sections. Section 1 is the introduction of vision-aided robotic welding, which emphasizes the importance of this review, the main development of robotic welding and the overall layout of this paper. Section 2 illustrates the pre-weld calibration, which includes vision sensor calibration and hand-eye calibration. Section 3 presents the positioning of SWP, of which methods are teach-playback and visual guidance. Section 4 reviews two vision sensing methods, namely active vision sensing and passive vision sensing. There are six active vision sensing methods based on laser structured light. And there are three passive vision sensing methods based on different welding features. Section 5 discusses the compensation and control in vision-aided robotic welding. Seam tracking algorithm and control strategy are summarized. Section 6 is the conclusion and future development. There is an obvious reference value for researchers to understand and apply these theories, methods and techniques to accomplish vision-aided robotic welding.

2. Pre-weld calibration

The pre-weld calibration consists of vision sensor calibration and hand-eye calibration. Vision sensor calibration is to solve the intrinsic and extrinsic parameters of the camera, and establish the relationship between the image coordinate system and the world coordinate system. Hand-eye calibration should calculate the homogeneous transformation matrix between the camera and the robot termination. The purpose of pre-weld calibration is that when vision sensor acquires the target information, the actual weld seam position can be calculated by the robot according to the target information and the calibration result. (Du et al., 2019).

Sharifzadeh et al. (2020) utilized a single planar calibration artefact to realize the hand-eye calibration between a 2D (two dimension) laser vision sensor and a robot. Zeng et al. (2019) proposed a calibration algorithm which decomposed the hand-eye matrix into its rotational matrix and polar coordinate matrix by the least square method. Liu et al. (2008) realized the simultaneous calibration of camera parameters and the hand-eye matrix.

The welding torch (or laser welding head) and vision sensor are rigidly mounted at the termination of the robot (Saeed and Zhang, 2007). In laser welding, there are two types for vision sensor system in terms of installation: (1) paraxial vision system (He et al., 2013), (2) coaxial vision system (Kim and Ahn, 2012). Paraxial vision system means that there is a relative position between the vision sensor and the laser welding head. Therefore, hand-eye calibration is necessary. Coaxial vision system means that the vision sensor and the laser welding head are coaxial installation. The camera coordinate system and the robot termination coordinate system can be considered as the same. Therefore, if the installation is coaxial, the hand-eye calibration can be omitted.

In arc welding, there is only paraxial vision system. This is because vision sensor can only be designed as paraxial installation relative to the welding torch. There is a relative position between the vision sensor and the welding torch. Therefore, hand-eye cal-

ibration and vision sensor calibration are essential for paraxial vision system. The basic idea of hand-eye calibration is to solve the matrix equation $AX = XB$ (Shiu and Ahmad, 1989). The methods of vision sensor calibration and hand-eye calibration are introduced in the following.

2.1. Vision sensor calibration

2.1.1. Camera model

The camera model can actually be represented as a pinhole model. Its imaging principle is the same as that of pinhole imaging. The vision sensor calibration is usually to solve the intrinsic and extrinsic parameters of the camera. The extrinsic parameters represent a rigid transformation from 3D world coordinate system to 3D camera coordinate system. The intrinsic parameters including focal length, principle point and pixel size represent a projective transformation from 3D camera coordinate into 2D image pixel coordinate (What is camera calibration?, 2020). As shown in Fig. 3.

Fig. 4 shows the schematic diagram of pinhole imaging. The coordinate (x_w, y_w, z_w) of a point in the world coordinate system $O_w-X_wY_wZ_w$ is transformed to the coordinate (x_c, y_c, z_c) in the camera coordinate system $O_c-X_cY_cZ_c$. The coordinate (x_c, y_c, z_c) projected into the image coordinate system $O_I-X_IY_I$ is (x_i, y_i) . The image is upside down relative to the real object according to the pinhole camera model (Zhang, 2000a). And the corresponding coordinate in the pixel coordinate system $O_p-X_pY_p$ is (x_p, y_p) .

The relationship between the world coordinate system and the camera coordinate system is described by Eq. (1):

$$\begin{pmatrix} x_c \\ y_c \\ z_c \end{pmatrix} = (R \ T) \begin{pmatrix} x_w \\ y_w \\ z_w \\ 1 \end{pmatrix} \quad (1)$$

Where, R and T are the rotation and translation matrixes, respectively. $[R, T]$ can represent the extrinsic parameters of the camera.

Fig. 5 (a) shows the illustration of intrinsic parameters (Shah and Aggarwal, 1996). P_0 is a point in the camera coordinate system $O_c-X_cY_cZ_c$. Then a line passing through P_0 and perpendicular to the plane $O_c-X_cY_c$ can be ensured. Furthermore, there is only one line like that. P_1 is the intersectional point between the line and the plane $X_cO_cY_c$. P_0P_1 is perpendicular to the plane $X_cO_cY_c$. P_2 is an image point in the image plane X_IY_I . According to $\triangle P_0P_1O_c \sim \triangle O_cO_I P_2$, the geometric and mathematical relationship between the camera coordinate system and the image coordinate system can be described by Eqs. (2)–(4):

$$x_i = fx_c/z_c \quad (2)$$

$$y_i = fy_c/z_c \quad (3)$$

$$z_c \begin{pmatrix} x_i \\ y_i \\ 1 \end{pmatrix} = \begin{pmatrix} f & 0 & 0 \\ 0 & f & 0 \\ 0 & 0 & 1 \end{pmatrix} \begin{pmatrix} x_c \\ y_c \\ z_c \end{pmatrix} \quad (4)$$

Where, f is the focal length, typically expressed in mm.

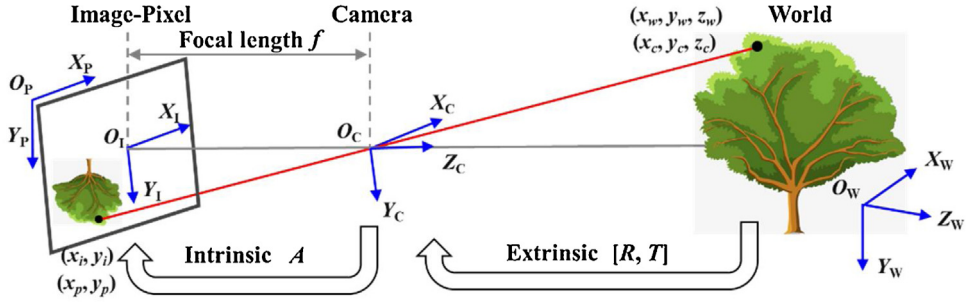


Fig. 4. The camera model and pinhole imaging principles.

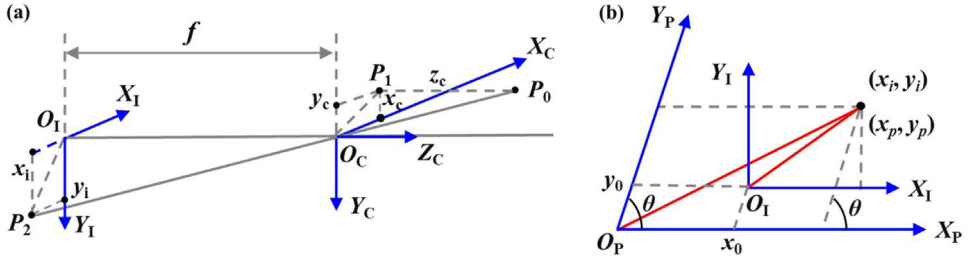


Fig. 5. The illustration of intrinsic parameters: (a) the camera coordinate projected into the image coordinate, (b) the relationship between the image coordinate and the pixel coordinate.

The relationship between the image coordinate system and the pixel coordinate system is illustrated in Fig. 5 (b).

$$x_p = x_0 + x_i/d_x - y_i \cot \theta / d_x \quad (5)$$

$$y_p = y_0 + y_i / (d_y \sin \theta) \quad (6)$$

$$\begin{pmatrix} x_p \\ y_p \\ 1 \end{pmatrix} = \begin{pmatrix} 1/d_x & -\cot \theta / d_x & x_0 \\ 0 & 1/\sin \theta d_y & y_0 \\ 0 & 0 & 1 \end{pmatrix} \begin{pmatrix} x_i \\ y_i \\ 1 \end{pmatrix} \quad (7)$$

Where, (x_0, y_0) represents the coordinate of O_I in the pixel coordinate system. d_x and d_y represent the size of pixel in world units. θ is the angle between the two axes in the pixel coordinate system.

Combining Eqs. (1)–(7), the relationship between the pixel coordinate system and the world coordinate system can be described by Eqs. (8)–(9).

$$\begin{pmatrix} x_p \\ y_p \\ 1 \end{pmatrix} = \begin{pmatrix} 1/d_x & -\cot \theta / d_x & x_0 \\ 0 & 1/\sin \theta d_y & y_0 \\ 0 & 0 & 1 \end{pmatrix} \begin{pmatrix} f & 0 & 0 \\ 0 & f & 0 \\ 0 & 0 & 1 \end{pmatrix} \begin{pmatrix} R & T \end{pmatrix} \begin{pmatrix} x_w \\ y_w \\ z_w \\ 1 \end{pmatrix} \quad (8)$$

$$\begin{pmatrix} x_p \\ y_p \\ 1 \end{pmatrix} = \begin{pmatrix} f/d_x & -f \cot \theta / d_x & x_0 \\ 0 & f / \sin \theta d_y & y_0 \\ 0 & 0 & 1 \end{pmatrix} \begin{pmatrix} R & T \end{pmatrix} \begin{pmatrix} x_w \\ y_w \\ z_w \\ 1 \end{pmatrix} \quad (9)$$

Where, camera calibration can be written as $K(x_p, y_p, 1)^T = A[R \ T](x_w, y_w, z_w, 1)^T$. K is the scale factor. A is the intrinsic parameter matrix and $[R \ T]$ is the extrinsic parameter matrix.

2.1.2. Camera calibration

2.1.2.1. Monocular vision calibration. Zhang et al. (Zhang and Huang, 2006) used a red/blue checkerboard with a checker size of 15×15 mm, as shown in Fig. 6 (a). When the checkerboard was illuminated by white light illumination, the black-and-white camera will see a uniform board. This is because the responses of

the black-and-white camera to red and blue colors are similar. As shown in Fig. 6 (b). When the checkerboard is illuminated by red or blue light, the black-and-white camera will see a regular checkerboard. This is because the red objects illuminated by red light are seen as white in the black-and-white camera. And the blue objects illuminated by red light are seen as black. As shown in Fig. 6 (c). The different positions and poses of the flat checkerboard are captured by a single camera. A total of ten images are used to obtain intrinsic parameters of the camera using Matlab toolbox, as shown in Fig. 7. The adopted camera is Dalsa CA-D6-0512 with a 25 mm lens (Fujinon HF25HA-1B). The size of each CCD pixel is 10×10 μm and the total pixels are 532×500 .

Zhang (2000b) printed a pattern and attached it to a planar surface. A few images of the model plane under different orientations are obtained by moving either the plane or the camera. The feature points in the image are detected. The five intrinsic parameters and all the extrinsic parameters are estimated by the closed-form solution. Finally, a nonlinear optimization technique based on maximum likelihood criterion is used to optimize all parameters including lens distortion parameters.

2.1.2.2. Binocular vision calibration. Peng et al. (2012) used two CCD cameras to construct a robot binocular vision system, of which function was developed by OpenCV. At first the checkerboard can be calibrated by the left and right camera, respectively. Then the intrinsic and extrinsic parameters will be obtained by the function of stereo vision calibration. Zhang et al. (Zhang and Yang, 2012) calibrated a binocular vision system by the commercial software Halcon10.0, which was superior to Matlab toolbox. Liu et al. (Liu and Xu, 2018) researched a tube-plate welding robot which adopted binocular vision calibration.

Chen et al. (Chen and Chen, 2010) fixed two same CCD cameras on the termination of the welding torch. The robot is Motoman XRC produced by YASKWA company and the camera type is WATEC-902H with a focal length of 4.8 mm. Image capture card CG-400 is produced by DaHeng Corporation. A mature method for camera calibration is adopted directly (Zhang, 2000b), and the calibration procedures are shown in Fig. 8 (b). The inter-

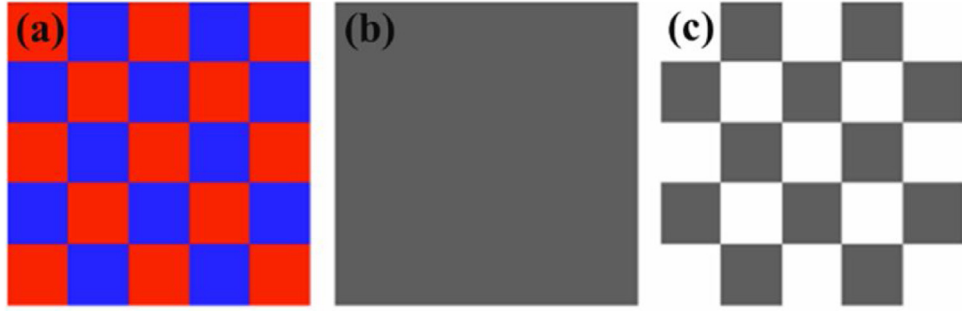


Fig. 6. Checkboard for calibration: (a) red/blue checkboard, (b) image with white light illumination, (c) image with red light illumination (Zhang and Huang, 2006).

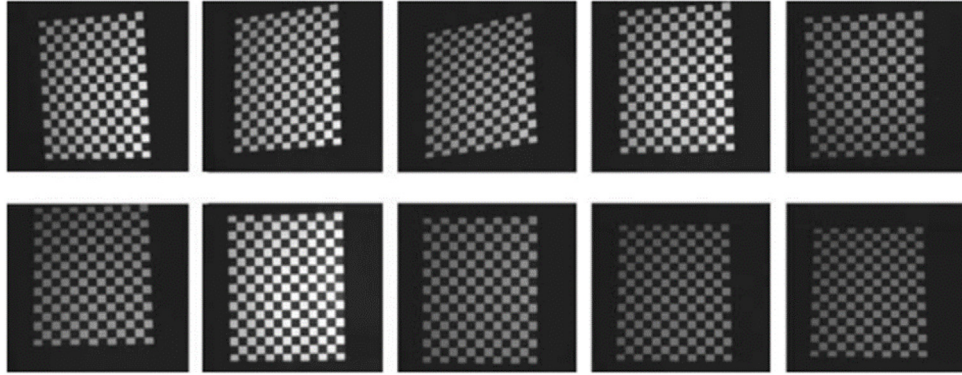


Fig. 7. Checkerboard images for camera calibration (Zhang and Huang, 2006).

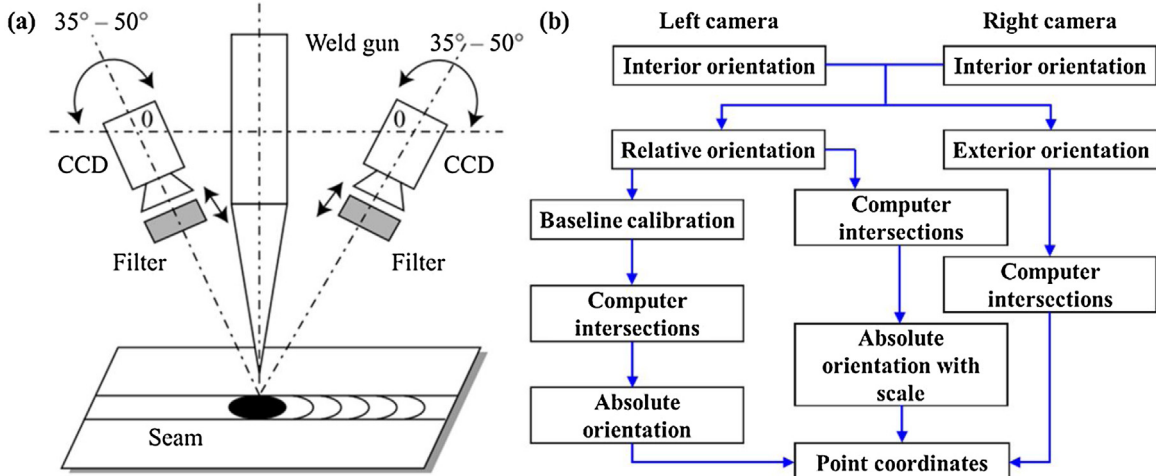


Fig. 8. Binocular vision calibration: (a) system setup, (b) calibration procedures (Chen and Chen, 2010).

nal and external parameters of the two cameras are calibrated by calculating the point coordinates.

2.1.2.3. Structured light aided vision calibration. Fan et al. (2016) and Qi et al. (2013) presented a camera calibration method based on laser structured light plane parameters for robotic welding. Fig. 9 (a) shows that a laser stripe is generated after the laser source projecting a structured light plane onto the planar grid target. The robot will move from one calibrating position to another with constraints so that two misaligned laser stripes can be generated. Four feature points which are generated onto the target can be extracted. And their coordinates will be utilized to solve the intrinsic and extrinsic parameters of the camera. The structured light plane parameters are also calibrated simultaneously, when the camera parameters

are calibrated by planar pattern calibration method (Feng et al., 2008). After the calibration of camera and structured light plane parameters, the 3D coordinate of feature points on multiple V-shape weld and zigzag weld can be measured. As illustrated in Fig. 9 (b) and (c).

2.2. Hand-eye calibration

There are two positional relationships between the camera and the robot (Schmidt and Wang, 2014): (1) the camera is positioned on the robot arm, namely, eye-in-hand. (2) the camera is positioned around the robot, namely, eye-to-hand. As a result of wide application of eye-in-hand in vision-aided robotic welding, this paper focuses on the hand-eye calibration of eye-in-hand.

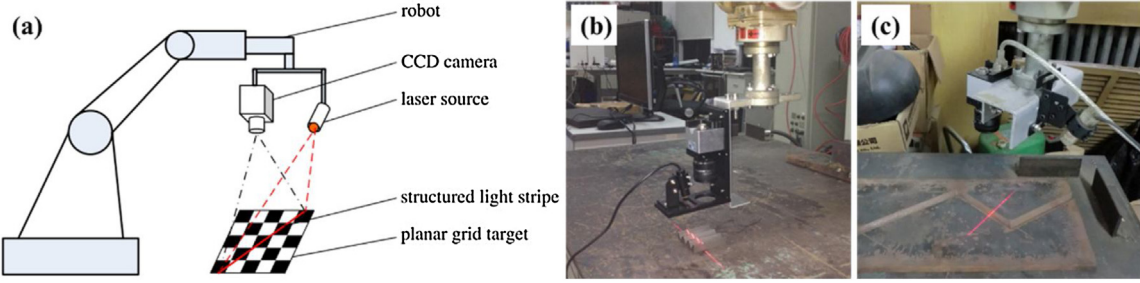


Fig. 9. Structured light vision measurement experiment after calibration: (a) system setup, (b) multiple V-shape weld, (c) zigzag weld (Fan et al., 2016; Qi et al., 2013).

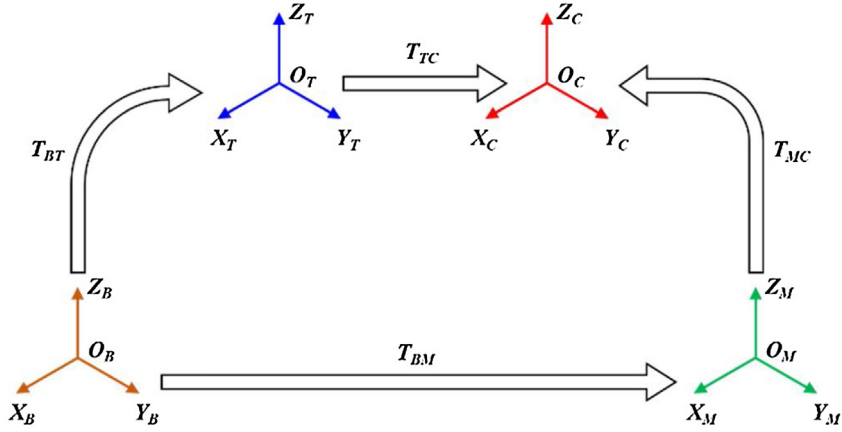


Fig. 10. Hand-eye calibration by three-coordinate measuring machine (Zhang et al., 2015a).

Zhang et al. (2015a) adopted three-coordinate measuring machine to calibrate the hand-eye relationship in the situation of robot welding an aero tube. Fig. 10 shows that O_T - X_T Y_T Z_T , O_C - X_C Y_C Z_C , O_M - X_M Y_M Z_M and O_B - X_B Y_B Z_B represent the robot termination coordinate system, camera coordinate system, measuring coordinate system and robot base coordinate system, respectively. T_{BT} can be directly obtained by robot control cabinet. T_{BM} and T_{MC} can be calculated by three-coordinate measuring machine according to four-point calibration method or three-point calibration method (Driels et al., 1993). The relationship among the four matrixes can be described by Eq. (10)–(11).

$$T_{BT}T_{TC} = T_{BM}T_{MC} \quad (10)$$

$$T_{TC} = (T_{BT})^{-1}T_{BM}T_{MC} \quad (11)$$

Where, T_{TC} is the rotary-translation matrix between the robot termination coordinate system and the camera coordinate system. T_{BT} is the rotary-translation matrix between the robot base coordinate system and the robot termination coordinate system. T_{BM} is the rotary-translation matrix between the robot base coordinate system and the measuring coordinate system. T_{MC} is the rotary-translation matrix between the measuring coordinate system and the camera coordinate system.

Sharifzadeh et al. (2020) solved the hand-eye calibration problem of a robot through a 2D laser vision sensor. Three orthogonal plane method can be replaced by a single plane method. As illustrated in Fig. 11 (a). The theoretical model of single plane calibration method by 2D laser sensor is shown in Fig. 11 (b). The purpose of hand-eye calibration is to define the homogeneous transformation T_{TC} that describes the relationship between the termination coordinate system and the camera coordinate system. Any observed point P_i in the camera coordinate system (2D profile) has a corresponding point P_B in the robot base coordinate system. The point in a 2D

profile is captured by a camera. The mathematical transformation is shown in the following equation.

$$P_B = T_{BT}T_{TC}P_i \quad (12)$$

Where, T_{BT} represents the homogeneous transformation matrix from the robot base coordinate system to the robot termination coordinate system. T_{TC} is the unknown hand-eye transformation matrix.

Dinham et al. (Dinham and Fang, 2009) adopted a low-cost method to calibrate the hand-eye relationship for arc welding robot with vision sensor. The calibration object with grid size 30×30 mm is utilized. The camera intrinsic and extrinsic parameter can be obtained using the Caltech Matlab toolbox (Bouguet, 2008). Fig. 12 (a) shows the related coordinate systems. Z_B represents the Z-axis of the robot base coordinate system. Z_T represents the Z-axis of the robot termination coordinate system. Z_C represents the Z-axis of the camera coordinate system. Z_W represents the Z-axis of the world coordinate system. The hand-eye transformation can be described as Eqs. (13)–(14).

$$T_{BW} = T_{BT}T_{TC}T_{CW} \quad (13)$$

$$T_{TC} = (T_{BT})^{-1}T_{BT}(T_{CW})^{-1} \quad (14)$$

Where, T_{BW} is the 4×4 homogenous transformation matrix from the robot base coordinate system to the world coordinate system. This matrix can be calculated by robot-world calibration, as shown in Fig. 12 (b). T_{BT} is the 4×4 homogenous transformation matrix from the robot base coordinate system to the robot termination coordinate system. This matrix is determined by nominal DH (Denavit-Hartenberg) (Corke, 2007) parameters. T_{TC} is the 4×4 homogenous transformation matrix from the robot termination coordinate system to the camera coordinate system. This matrix is hand-eye transformation matrix. T_{CW} is the 4×4 homogenous transformation matrix from the camera coordinate system to the

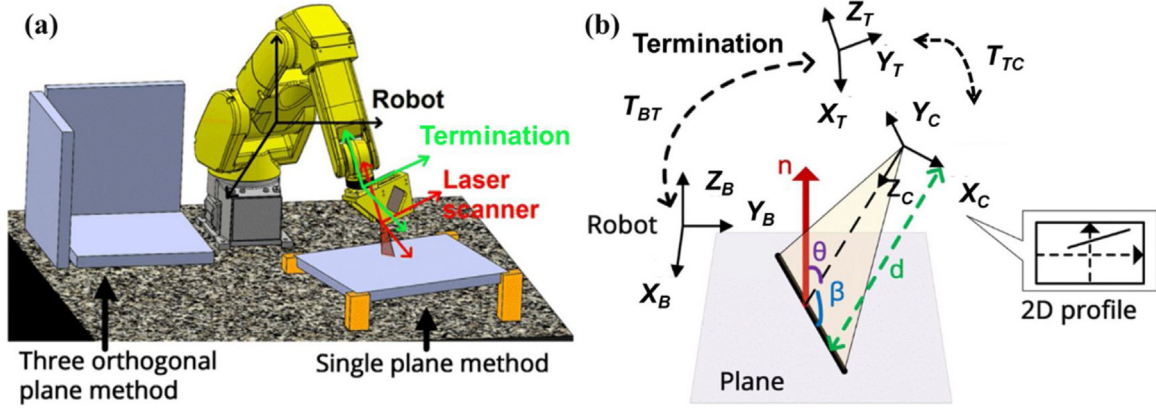


Fig. 11. Hand-eye calibration: (a) the single plane calibration method, (b) the theoretical model of single plane calibration method (Sharifzadeh et al., 2020).

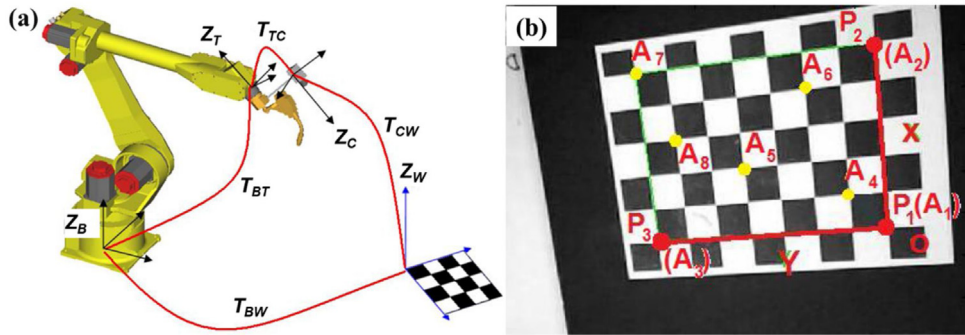


Fig. 12. Hand-eye calibration: (a) the diagram of the relationship between the four coordinate systems, (b) the robot-world calibration (Dinham and Fang, 2009).

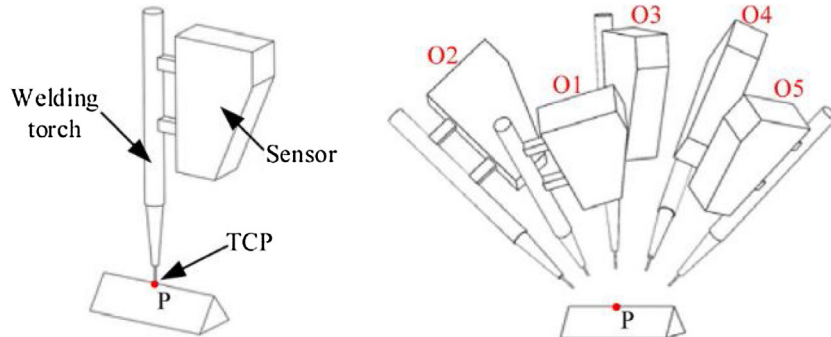


Fig. 13. Five-point calibration procedure (Zou and Chen, 2018).

world coordinate system. This matrix can be obtained by vision sensor calibration.

The hand-eye calibration process can be achieved by moving the robot through 15 positions. And the image of the calibration object can be captured at each robot position. Meanwhile, T_{TC} is calculated by Eq. (14). The rotation component of every T_{TC} is converted to its Euler Angle equivalent. The average of 15 sets of Euler Angles is then converted back to its 3×3 rotation matrix format. This value is then taken to be the rotation component of T_{TC} . Similarly, the translational components are average, and the average are taken as the translation component of T_{TC} .

Zou et al. (Zou and Chen, 2018) even used the five-point calibration procedure of the robot to accurately calculate the relationship between the TCP (Tool center point) and the robot base coordinate system. These calibration points can be evenly distributed within the robot's workspace. For each point, its position in the base coordinate system can be obtained. This operation is benefi-

cial to improve the accuracy of hand-eye calibration. As shown in Fig. 13.

Table 1 shows the common methods of vision sensor calibration and hand-eye calibration. The calibration works are the premise of vision-aided robotic welding. Monocular vision calibration is simple and easy to realize. However, more calibration pictures are necessary. Binocular vision calibration owns wide measuring range and 3D calibration information can be measured. However, the mathematical model of calibration is complicated. Structured light aided vision calibration owns the advantages of high accuracy and anti-interference capability. Meanwhile, this calibration method is more widely used than the previous two calibration methods. However, the calibration of structured light plane is needed. Hand-eye calibration is to solve the position relationship between the sensor and the termination coordination system of a robot. Three-coordinate measuring machine can measure the required transformation matrix. And the robot doesn't need to move and

Table 1

The common calibration methods.

Calibration methods	Authors	Calibration object	Methods	Merits	Demerits
Vision sensor calibration	• Monocular vision calibration	• Zhang et al. (Zhang and Huang, 2006) • Zhang (2000b)	• A red/blue checkerboard • A printed pattern paper is attached to a planar surface	• Matlab toolbox • The feature points are detected when the plane or the camera is moved	• Simple and easy to realize • More calibration pictures are necessary
	• Binocular vision calibration	• Peng et al. (2012) • Zhang et al. (Zhang and Yang, 2012)	• Plane chessboard calibration template • A standard calibration plate (100 × 100 mm)	• OpenCV • Halcon10.0 software	• Wide measuring range; 3D calibration information can be measured • The mathematical model of calibration is complicated
	• Structured light aided vision calibration	• Fan et al. (2016) • Qi et al. (2013)	• A planar grid chessboard • Planar grid target	• Four points calibration method • A line-feature-based calibration method	• High accuracy and anti-interference capability • The calibration of structured light plane is needed
Hand-eye calibration	• Three-coordinate measuring machine aided calibration	• Zhang et al. (2015a)	• Not required	• Four-point or three-point calibration method	• The robot doesn't need to move; less user interaction • Expensive and time consuming
	• 2D laser vision sensor aided calibration	• Sharifzadeh et al. (2020)	• Not required	• A single plane calibration method	• Small angles leading to non-convergence can be avoided • A single plane artefact is needed
	• Vision sensor aided calibration	• Dinham et al. (Dinham and Fang, 2009)	• A calibration chessboard with grid size 30 × 30 mm	• Matlab toolbox	• A low-cost, direct and common method • The calibration error is within ± 1 mm

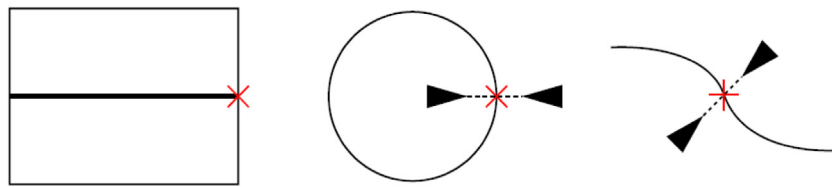


Fig. 14. The definition of SWP (Wei et al., 2010).

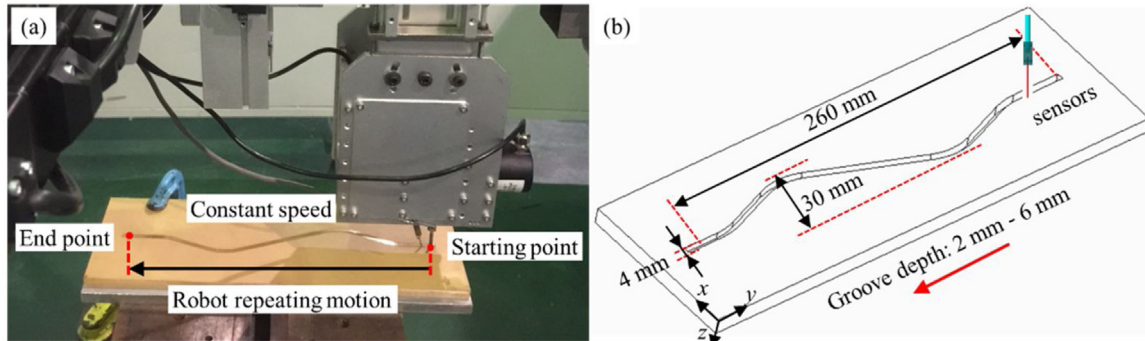


Fig. 15. Detection in a wavy groove of square weldment: (a) robot repeating motion, (b) wavy groove (Lei et al., 2020a).

user interaction is less. The demerits of this calibration method are that the measure device is expensive and the operation is time consuming. 2D laser vision sensor can avoid the non-convergence of calibration leaded by small angles. And the calibration accuracy is high. However, a single plane artefact is needed. Vision sensor is a low-cost, direct and common method. However, the calibration error is within ± 1 mm. In the future, structured light aided vision calibration and 2D laser sensor aided calibration are probable the future directions due to their high accuracy.

3. The positioning of SWP

SWP is start welding point and it also can be called IWP (initial welding point). This point is the first welding position. The SWPs are always some points with obvious features, such as the corners, the intersection points of weldment boundary and seam (Chen and Chen, 2010), intersection points of seam and connecting line between specific points on the marks in the case of flat flange and space curve seam (Wei et al., 2010). As shown in Fig. 14. The positioning of SWP is one of the key factors influencing robotic welding quality. Furthermore, the automatic identification and guidance of SWP are the premise of intelligent robotic welding. Generally, the positioning of SWP mainly includes teach-playback and visual guidance.

3.1. Teach-playback

Currently, the teach-playback mode is still adopted for welding robots to weld fillet joint, butt joint and lap joint etc. Especially in the case of low welding accuracy, teach-playback with the advantage of repeating predefined actions is an irreplaceable mode. During operation, the welder moves the welding torch next to a weldment by physically hand-guiding the robot. Once the welding point is confirmed, the welder records the position and determines the welding parameters. After all necessary welding points are recorded, the welder can play back the programmed weld seam trajectory (Yaskawa Motoman: Teaching Technology for Welding Robots, 2020).

It is necessary for welding robot to record its SWP and EWP (end welding position) for weld seam tracking in teach-playback

mode. This is because the moving trajectory and direction should be told to the robot. Lei et al. (2020a) adopted two tactile sensors to detect the curve weld trajectory. The coordinates of start point and end point can be recorded by the robot. The robots will move at a constant speed according to the linear motion program. As shown in Fig. 15. Xu et al. (2017) developed a robotic GMAW (gas metal arc welding) system for seam tracking based on a purpose-built vision sensor. The SWP and EWP in fillet joint are taught, as illustrated in Fig. 16 (a). Piecewise interpolation algorithm is utilized and the accuracy verification tests are conducted. As shown in Fig. 16 (b).

Although teach-playback mode can meet several welding requirements, the operator must learn a robot specific programming language and enter these instructions in the teach pendant (Robotic welding issues and challenges, 2020). Moreover, the robots in this mode have a poor adaptability to multi-varieties and small-batch weldments. Offline programming is also a technology that can realize the positioning of SWP. The trajectory of robot can be pre-planned by offline programming in a robotic simulation software (. Mineo et al. (2016) researched a new software solution that enabled flexible trajectory planning to be accomplished for the inspection of complex curved surfaces. However, both teach-playback and offline programming are unable to perceive and cope with the welding state of the weldment. Therefore, the positioning of SWP by visual guidance has attracted a lot of attention.

3.2. Visual guidance

3.2.1. The recognition of SWP

SWP is usually recognized by vision sensor or laser vision sensor. Li et al. (2015b) adopted a passive vision sensor to recognize the SWP of large-diameter pipeline. The target regions can be obtained by image segmentation and removal of small false regions based on pulse-coupled neural network. One of the solid joints can be recognized from the local image and its centroid can be extracted. The centroid will be regarded as SWP. Wei et al. (2010) proposed a recognition method of SWP with a single camera and two positions. An improved Harris Algorithm can be used to extract the corner point of a certain position, and grey scale scanning method can be utilized to identify the SWP of flat flanges. Chen et al. (2006) used a single camera and an improved template match technology to

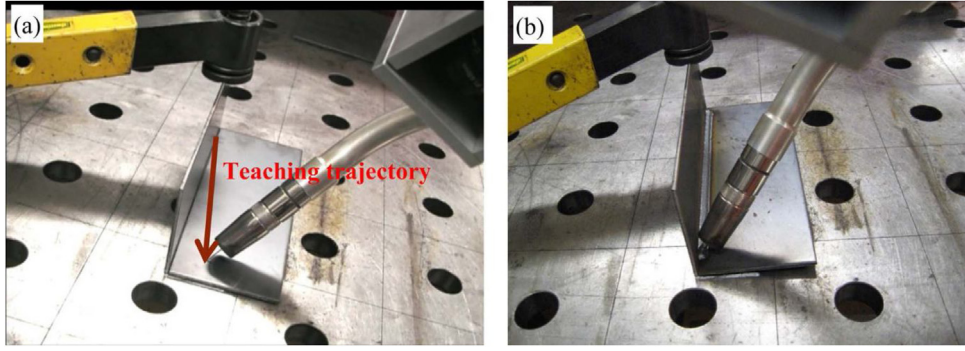


Fig. 16. Weld seam tracking for a fillet joint: (a) teaching trajectory, (b) welding results (Xu et al., 2017).

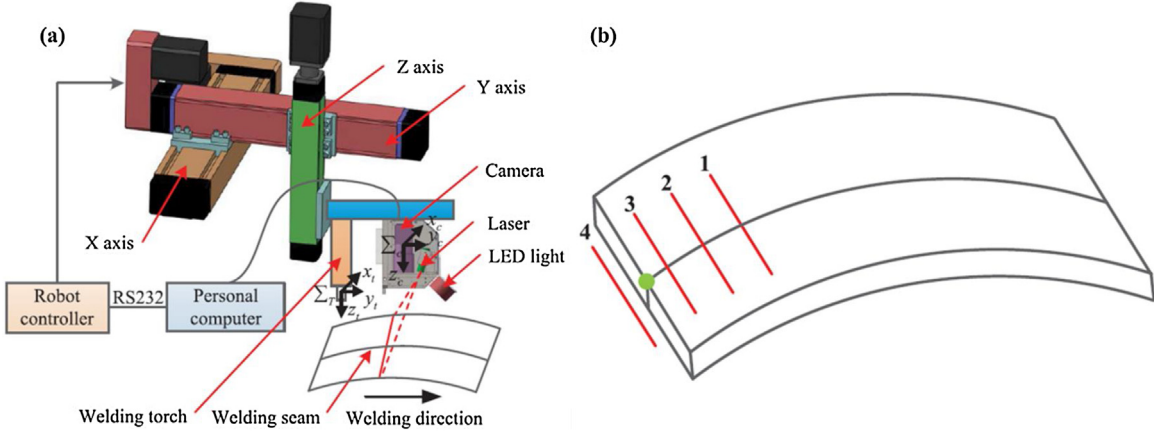


Fig. 17. The recognition of SWP by laser vision sensor: (a) system setup, (b) the position of laser stripe during moving (Fan et al., 2019a).

locate SWP in the pixel level. Polynomial interpolation technology of pixel can be applied to subdivide the pixel coordinates, which can obtain a higher precision. Zhu et al. (2005) adopted the two-step pattern match method. The error points can be wiped off during the global pattern match stage and the SWP can be recognized by adjusting the search area during the local pattern match stage in the area of near the SWP. Fan et al. (2019a) established a seam tracking system based on laser vision sensor. As shown in Fig. 17 (a). The intersection of the laser stripe and the weld seam is regarded as the image feature point. As illustrated in Fig. 17 (b). The feature point can be extracted by three steps: profile extraction, random sample consensus, line extraction and feature point computation.

3.2.2. Calculating the coordinates of SWP

Fan et al. (2019b) illustrated the detailed steps to calculate the coordinates of SWP. Fig. 18 shows the center line S_1 of the weld seam and the laser stripe L_1 . B_1 is the boundary line of the weldment. p_1 is the feature point of laser stripe. p_2 is the initial point. p_3 is an intermediate transition point, which is located on the laser stripe. The image coordinates of p_1 and p_2 can be extracted by image process algorithm. The image coordinates of p_3 can be calculated by Eq. (15).

$$\begin{cases} u_3 = u_2 \\ v_3 = v_1 + (u_2 - u_1)\tan\theta \end{cases} \quad (15)$$

Where, θ is the angle between B_1 and L_1 .

According to the pinhole model of camera and the equation of laser structured light plane, the 3D coordinates of p_3 (x_{c3}, y_{c3}, z_{c3}) in camera coordinate system can be expressed by Eq. (16). Based

on the hand-eye relationship, the 3D coordinates of p_3 (x_{t3}, y_{t3}, z_{t3}) in the termination coordinate system can be calculated by Eq. (17).

$$\begin{cases} z_{c3} = ck_x k_y / (k_x k_y + ak_y (u_0 - u_3) + bk_x (v_0 - v_3)) \\ x_{c3} = z_{c3} (u_3 - u_0) / k_x \\ y_{c3} = z_{c3} (v_3 - v_0) / k_y \end{cases} \quad (16)$$

Where, p_3 (u_3, v_3) is image coordinates. k_x and k_y are the magnification factors in x-axis and y-axis directions, respectively. And (u_0, v_0) is its principal point.

$$\begin{pmatrix} x_{t3} \\ y_{t3} \\ z_{t3} \\ 1 \end{pmatrix} = \begin{pmatrix} n_x & o_x & a_x & p_x \\ n_y & o_y & a_y & p_y \\ n_z & o_z & a_z & p_z \\ 0 & 0 & 0 & 1 \end{pmatrix} \begin{pmatrix} x_{c3} \\ y_{c3} \\ z_{c3} \\ 1 \end{pmatrix} = T_{TC} \begin{pmatrix} x_{c3} \\ y_{c3} \\ z_{c3} \\ 1 \end{pmatrix} \quad (17)$$

Where, $n = [n_x, n_y, n_z]^T$ is the direction vector of x_c in the termination coordinate system, and $o = [o_x, o_y, o_z]^T$ is the direction vector of y_c in the termination coordinate system, and $a = [a_x, a_y, a_z]^T$ is the direction vector of z_c in the termination coordinate system, and $p = [p_x, p_y, p_z]^T$ is the position vector of the original point in the termination coordinate system. T_{TC} is the transformation matrix between the termination coordinate system and the camera coordinate system. The reason why calculates the coordinate of p_3 is that it is very hard to directly solve the coordinate of p_2 . Meanwhile, the coordinate of p_3 can be calculated in each coordinate system. Then the distance between p_3 and p_2 in the image coordinate system can be computed, shown in Fig. 18 (b). The distance between p_3 and p_2 in the camera coordinate system can also be calculated. In the end, the distance between p_3 and p_2 in the termination coordinate system can be expressed.

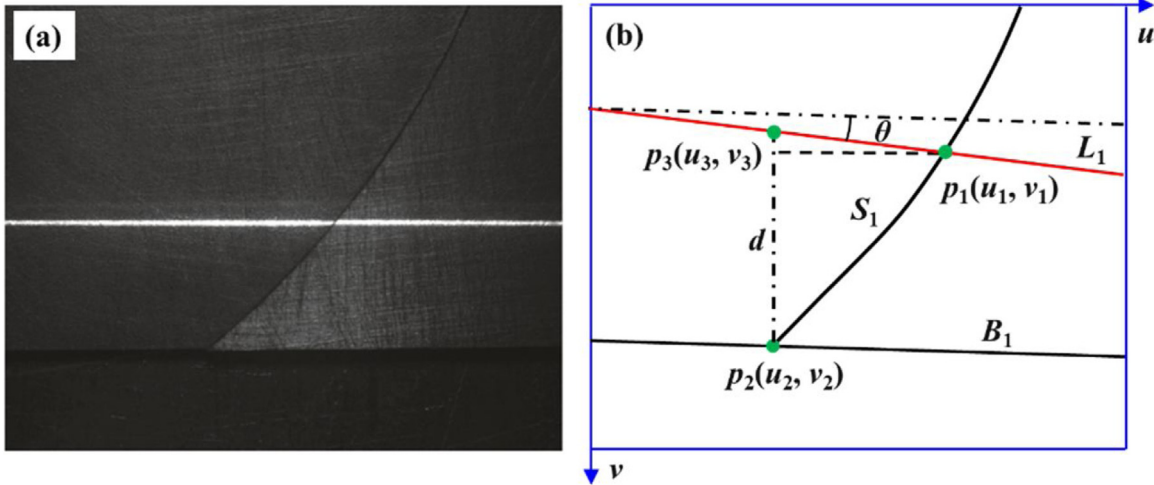


Fig. 18. the relationship between the feature point of laser stripe and the initial point (a) the laser stripe image (b) geometric diagram (Fan et al., 2019b).

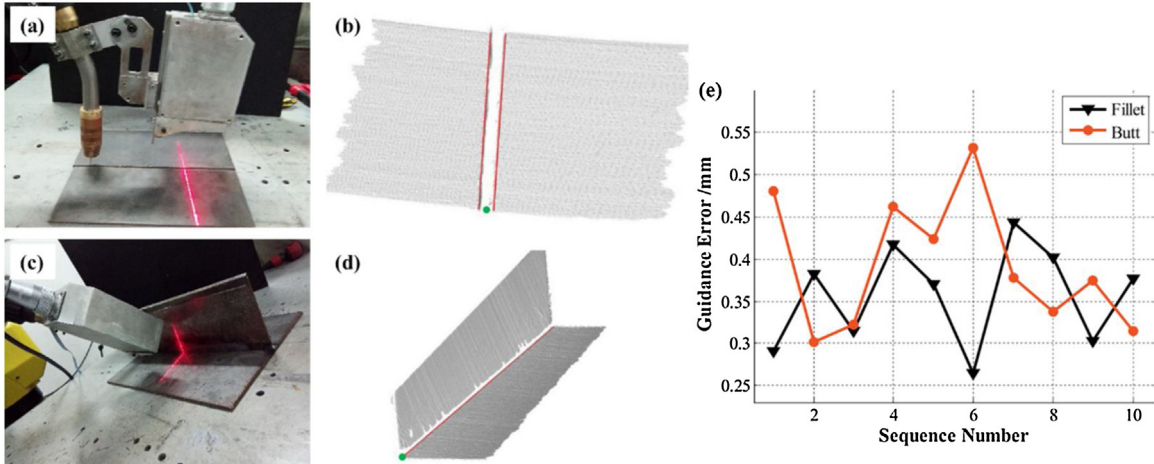


Fig. 19. Ten sets of SWP guidance test: (a) butt weld seam, (b) SWP extraction in butt weld seam, (c) fillet weld seam, (d) SWP extraction in fillet weld seam, (e) guidance error (Xiao et al., 2019).

Xiao et al. (2019) used a laser vision sensor to obtain 3D point cloud data of weld seam reconstruction. Through point cloud process, the equations and the SWP of weld seam can be obtained. Ten sets of SWP guidance precision experiments can be performed on butt weld seam and fillet weld seam, shown in Fig. 19 (a) and (c), respectively. Fig. 19 (b) and (d) shows that the edges of weld seam are marked as red line. The SWPs are in green dots. Fig. 19 (e) shows the guidance test results and the guidance error is less than 0.6 mm. It can meet the actual welding requirements.

3.2.3. Guiding control of SWP

PID (Proportional-integral-derivative) controller has the advantages of simple, stable and reliable. It is often used as SWP guidance controller. The SWP controller is designed to make welding torch align with the SWP based on position-based visual serving method (Fan et al., 2019a). The incremental type of PID controller can be described by Eq. (18).

$$\begin{cases} \Delta u(k) = P_e [K_p [e(k) - e(k-1)] + K_i e(k) + K_d [e(k) - 2e(k-1) + e(k-2)]] \\ u(k) = u(k-1) + \Delta u(k) \end{cases} \quad (18)$$

Where, P_e is the number of pulses corresponding to 1 mm. This means that how many pulses are required for the actuator to move 1 mm. K_p , K_i and K_d are the three parameters of the PID controller. The increment $\Delta u(k)$ is the output pulse at sample cycle k .

The 3D coordinates of SWP are regarded as the reference value. The 3D coordinates of feature point can be extracted by the image feature detection algorithm. The rotary encoder can be considered as a sensor. When the 3D coordinates of feature point deviates from the 3D coordinates of SWP, the deviation distance between the SWP and the feature point can be calculated by the rotary encoder. Meanwhile, the deviation distance can be converted into the number of pulses. The pulse signal will be sent to the PID controller. The guiding of SWP will not finish until the deviation distance is smaller than a threshold value. As shown in Fig. 20.

Nele et al. (2013) developed a three-axis welding torch moving system. The x-axis with a 3-mm stroke can be driven by a DC motor. The y-axis and z-axis motion can be provided by two stepper motors, allowing a travel of 500 mm. The algorithm of automatic positioning SWP can be programmed in Labview environment.

Fang et al. (2013) proposed the principle of two close-loop control systems of positioning SWP, as shown in Fig. 21. The target image feature f_4 is the reference signal in the first close-loop control system. The current image feature f_c is the feedback signal in the second close-loop control system. Both are computed in the computer using the seam images captured from the camera. The time for computing the target or the current image feature is determined by a soft switch. The switch is realized in the PLC (programmable logic controller). When the switch is put on the point p_r , the tar-

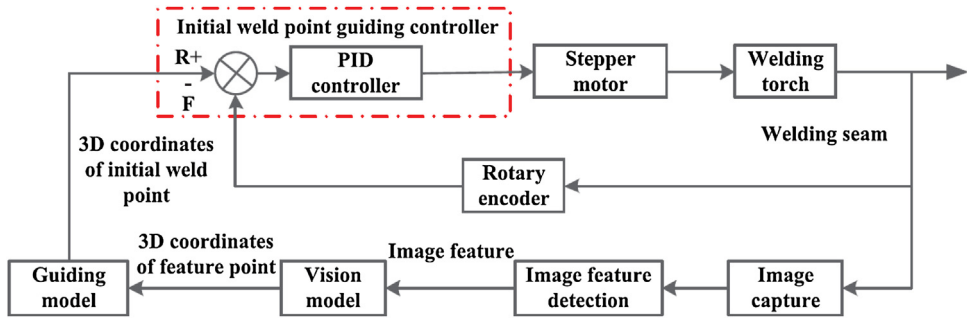


Fig. 20. The principle of SWP guidance control (Fan et al., 2019a).

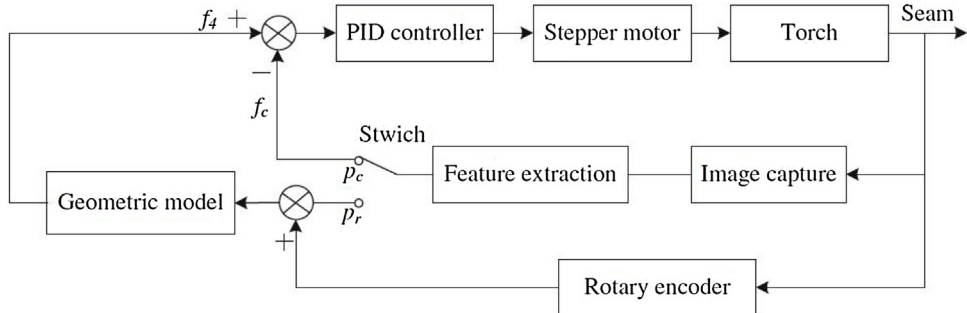


Fig. 21. The principle of two close-loop control system (Fang et al., 2013).

get image feature is computed based on the target seam image, and the position of the torch is read from the encoder and the geometric model. On the other hand, when the switch is put on the point p_c , the current image feature is computed based on the current seam image. Therefore, the deviation signals between f_4 and f_c can be calculated. The incremental PID controller is used to correct the torch based on the deviation signals. The aligning process can be called the “look-and-move” control model.

There are two common positioning methods for SWP. Namely, teach-playback and visual guidance. Table 2 shows the merits and demerits of the positioning methods for SWP. Teach-playback is a simple, low-cost and low barrier to entry. It is widely used in small and medium-sized enterprises. However, it is hardly to perceive the state of the weldment. Thus, this method has a poor adaptability to multi-varieties and small-batch weldments. Moreover, the positioning accuracy depends on the operator's experience.

Visual guidance can perceive and cope with the weldment. The recognition, calculation and guidance control are the basic stages of visual positioning for SWP. This method owns a higher positioning accuracy and can realize autonomous positioning. The image processing, 3D point cloud and control principle are involved in this method. Although the implementation of this method is complex, visual guidance is probable the future direction of vision-aided robotic welding.

4. Vision sensing

Not only can the positioning of SWP adopt vision sensing, but also weld seam tracking can employ vision sensing. Depending on the light source, the vision sensing can be divided into two types: (1) active vision sensing, (2) passive vision sensing. Active vision sensing usually takes laser structured light as auxiliary light source. Passive vision sensing directly uses ambient or arc light as the background light source. Active vision sensing can select the intensity, incident angle, and the wavelength of light, of which application is very wide. On the contrary, passive vision sensing is more proper in detecting the molten pool, welding layer and swing arc. This is

because the light generated by welding can be regarded as the light source. Therefore, the two sensing methods have their merits and demerits.

The weld seam geometry information can be obtained by both active vision sensing and passive vision sensing (Pinto-Lopera et al., 2016). Furthermore, in order to observe the molten pool, spatter, plasma and other welding characteristics, it is necessary for active and passive vision systems to own an optical band-pass filter with a narrow bandwidth (Muhammad et al., 2018). The spectrum of narrow optical band-pass filter should be determined by the light from electric arc or molten pool. According to the weld type and joint form, it is necessary to determine which type of laser structured light is suitable for active vision sensing (Xu et al., 2007a). Image processing algorithm can reduce the difficulty of extracting weld feature information after active vision sensing technology being adopted. Passive vision sensing is usually utilized in the situation of high contrast between the molten pool and other objects in the scene (Xiong et al., 2013).

4.1. Active vision sensing

4.1.1. Single-line laser

Fan et al. (2017) developed an automatic recognition system of weld type based on support vector machine (SVM). A laser stripe can be formed when laser intersects with the weldment. The center contour of laser stripe on 6 different weld seam types can be extracted, such as symmetric V groove, left V groove, right V groove, I groove, left lap groove and right lap groove. The weld type recognition can be divided into two parts, input feature vector computation and modeling method based on SVM. Liu et al. (2006) projected a single-stripe laser to the groove in the welding process. The noises can be separated by wavelet transforms and the width, center and cross-section of the groove can be extracted. The whole processing time is 250 ms (millisecond), basically meeting the requirement of real-time tracking. Lü et al. (Lü et al., 2018) researched the seam images with a single-line laser stripe under different types of groove. The ridge line tracking and direction tem-

Table 2

The merits and demerits of the positioning methods for SWP.

Positioning Methods	Authors	Merits	Demerits
The positioning for SWP	• Teach-playback	• Simple, low-cost and low barrier to entry	• The accuracy depends on the operator's experience
	• Visual guidance	The accuracy is very high	• The implementation procedure is complex

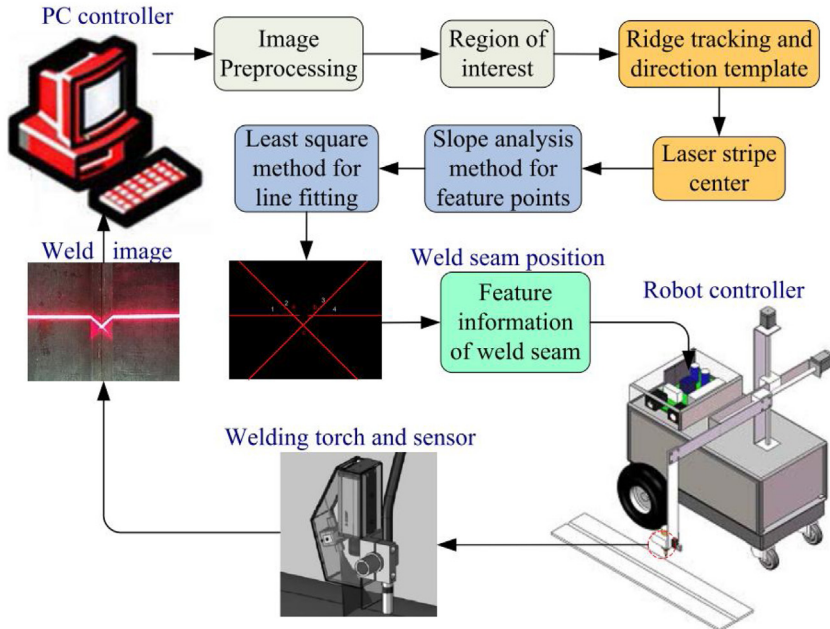


Fig. 22. The flow diagram of robotic welding based on single-line laser vision (Gu et al., 2018).

plate suitable for laser stripe center extraction can be used to obtain the weld groove information during robot movement. Fig. 22 shows the flowchart of robotic welding based on single-line laser vision. Reichert et al. (Reichert and Peterson, 2007) demonstrated the feasibility of using laser vision profiles and topography to classify and measure the weld size of RSW (resistance spot weld) fractures. The size of RSW fractures obtained by laser contour measurement is a good correlation with the measurement result of manual caliper. Saeed et al. (Saeed and Zhang, 2007) even used a calibrated CCD camera and a single-line laser to extract the surface information for the depth of molten pool from the captured images. Li et al. (2018) even used a vision sensing system based on single-line laser to monitor the oscillation of weld pool. The oscillation frequency of weld pool and the fluctuation amplitude of centroids of laser pattern can be extracted.

4.1.2. Cross-lines laser

Single-line laser owns several advantages in the detection of straight-line weld. However, it is unsuitable for detecting T-shaped and Cross-shaped weld seams etc. On the contrary, when cross-lines laser is projected on these weldments, the weld feature information formed by cross-lines laser is larger than that formed by single-line laser. According to the triangulation measuring method, cross-lines laser aided vision can not only detect the weld width but also the weld height. Lei et al. (2020b) established the linear relationship between WHVV (welding height variation value) and ICCL (intersection coordinate of cross-lines laser) in tube-to-tubesheet welding. The WHVV is mainly influenced by the thermal deformation of tubesheet. The ICCL between the current tube and the referential tube can be extracted and calculated, therefore, the

WHVV can be calculated. Zhang et al. (2014a) realized a weld line location for mobile platform via a CSL (cross structured light) and spatial-temporal cascaded HMMs (hidden Markov models), shown in Fig. 23 (a). The problem of the stripe extraction can be formulated in a S-HMM (spatial HMM) framework. The located ROIs in video frames can be fed to a designed T-HMM (temporal HMM) for tracking weld line. Fig. 23 (b) illustrates the flowchart and principle. Cross-lines laser is also used in 3D reconstruction (), the detection of medium steel plate flatness (), T-intersection weld lines (Zhang et al., 2014b) and aperture (Li et al., 2010) etc.

4.1.3. Multi-lines laser

Compared with single line laser and cross-lines laser, multi-lines laser can be more appropriate for seam tracking of complex welds such as space curve. When the points are not continuous or interfered by arc and flash, the more valuable position information can be presented by multi-lines laser. There are many types of multi-lines laser. Zhang et al. (2018a) realized the identification of the deviation of seam tracking for wall-climbing robot based on 3-lines laser structured light, shown in Fig. 24 (a). Zou et al. (2018a) designed a 3-lines laser vision sensor to locate the coordinates of feature point of butt welds, lap welds and complex curve welds. Shao et al. (2018) utilized a green laser stripe and two red laser stripes to measure the 3D position of the space weld seam of narrow butt joint, shown in Fig. 24 (b). Sung et al. (2009) overcame the accurate problem of detecting the joint for high-speed welding with a 5-lines laser vision sensor. Ma et al. (Ma and Zhang, 2011) developed a GMAW observation system based on 5-lines laser vision to monitor the 3D weld pool. (et al. (2005) made use of 3-lines laser structured light to form a triangular structure light shape. The weld

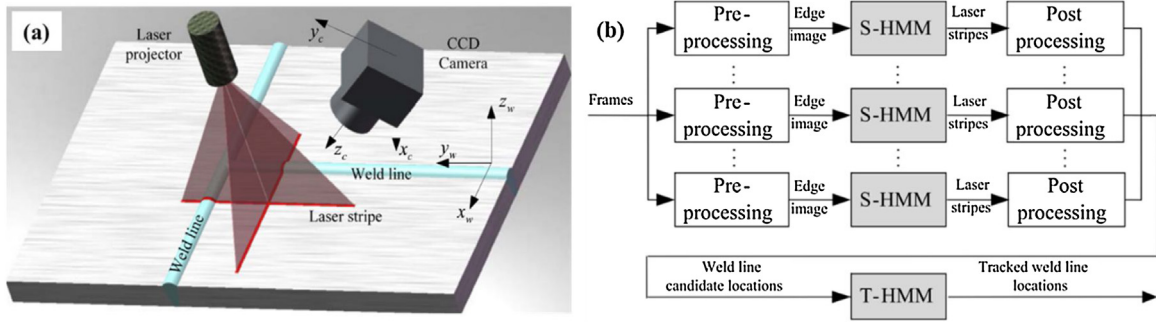


Fig. 23. The relevant illustration: (a) the structure of CSL projector and CCD camera on weld lines, (b) the flowchart of tracking weld line with STC-HMMs (Zhang et al., 2014a).

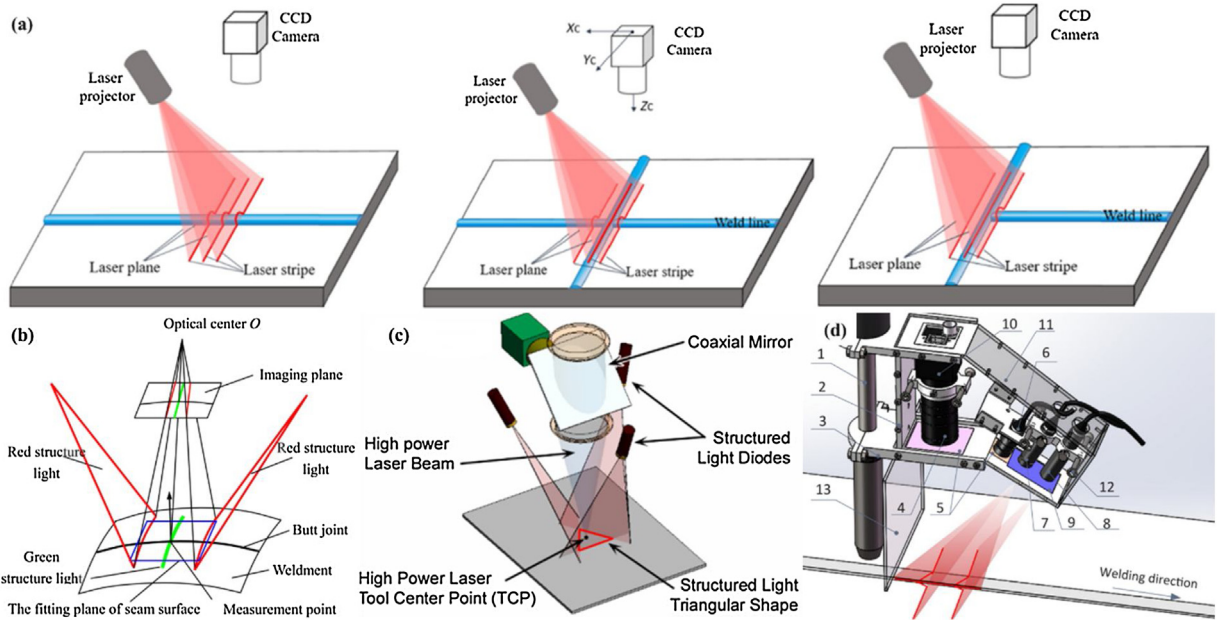


Fig. 24. The types of multi-lines laser: (a) 3-lines laser for straight, T-shaped and Cross-shaped weld seams, (b) a green and two red laser lines, (c) triangular shape structured light, (d) a single line and cross-lines laser (Zhang et al., 2018a; Shao et al., 2018; Iakovou et al., 2005; Guo et al., 2019).

seam tracking and post-weld inspection can be realized by this specific design, shown in Fig. 24 (c). Guo et al. (2019) even presented an innovative multi-functional monocular vision sensor with single-line laser and cross-lines laser. The cross-section dimension of the welding groove and the height of welding torch perpendicular to the upper surface of weldment can be detected, shown in Fig. 24 (d).

4.1.4. Grid-lines laser

Single-line laser or multi-lines laser can't provide the completed information for the finished weld seam, and can't detect the next weld seam after the based layer welding has been finished. Grid-lines laser contains multiple horizontal and vertical intersecting lines. It is feasible to obtain the intersections and carry on further treatment. Zhang et al. (2017) realized weld seam sensing in multi-layer and multi-pass welding with grid-lines laser structured light. A robust algorithm can be adopted to extract the feature points from the distorted grid-lines structured light. It can detect the previous weld beads and predict the following welding position of the next layer. As shown in Fig. 25 (a). Jia et al. (2019) projected a 9×9 orthogonal grid-lines laser on the weld surface. The 3D information of the weld surface can be reconstructed by the laser-photo hybrid method rather than the continuous image acquisition by the line-laser sensor. It is shown in Fig. 25 (b). Kovacevic et al. (Kovacevic and

Zhang, 1996) even projected a specific grid-lines laser onto the weld pool. The surface shape of 3D weld pool can be clearly displayed by the specular reflection and the skeleton of the specular reflection can be extracted by an advanced image processing technology.

4.1.5. Dot matrix laser

The dot matrix laser owns the advantages of wide coverage and high sensitivity. The variation of weld feature information can be reflected by the difference between the adjacent laser dots. Zhang et al. (2013) projected a 19×19 dot matrix laser on the weld pool region in a stainless steel pipe welding. The reflection from the weld pool surface will be intercepted by the imaging plane. As shown in Fig. 26 (a). An analytic reconstruction algorithm for the 3D weld pool surface has been introduced in detail. The error of boundary reconstruction at the simulation of the bench mark is 0.11 %, and the error of height reconstruction at the maximum height is 0.024 %. Song et al. (Song and Zhang, 2007) established the corresponding relationship between the reflection points and their projection points in a plate welding with the use of dot matrix laser. Moreover, the error of the 3D GTAW (gas tungsten arc welding) weld pool surface measurement system has been analyzed (Song and Zhang, 2009). As shown in Fig. 26 (b). Saeed et al. (2004) also utilized dot matrix laser and a CCD camera to observe the molten reflection pat-

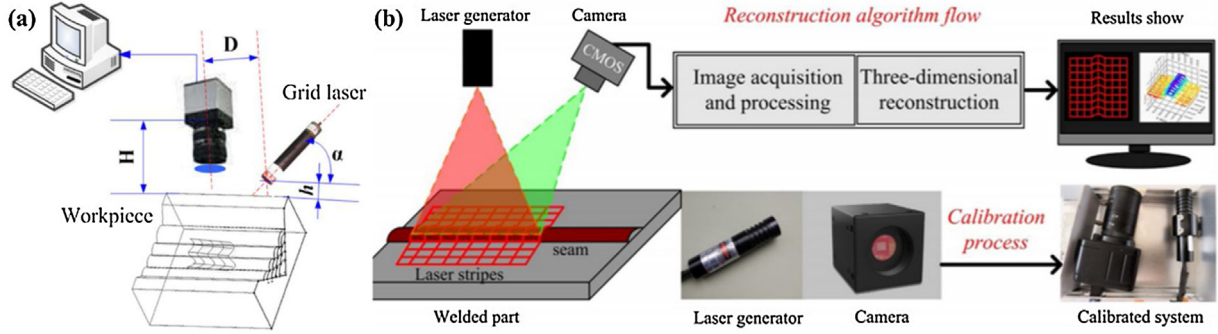


Fig. 25. Weld seam sensing system based on grid-lines laser: (a) multi-layer and multi-pass welding, (b) 3D reconstruction weld (Zhang et al., 2017; Jia et al., 2019).

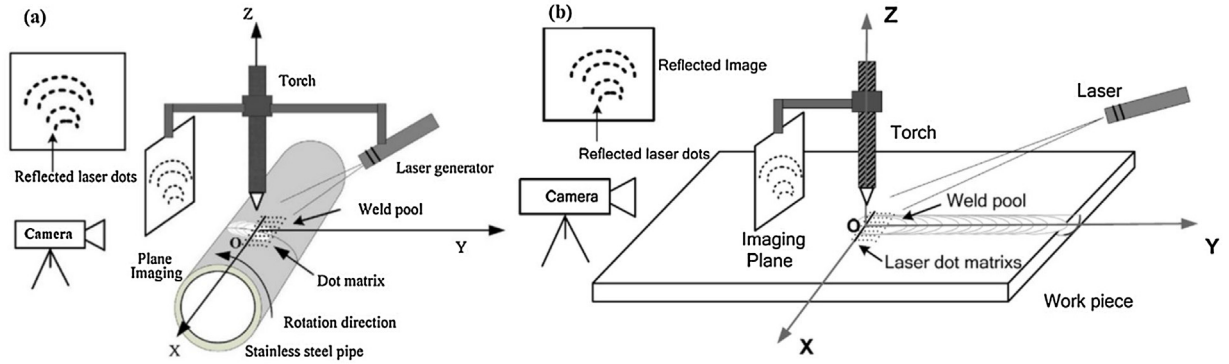


Fig. 26. The measuring diagram of vision sensing based on dot matrix laser: (a) pipe welding, (b) plate welding (Zhang et al., 2013; Song and Zhang, 2007).

terns. The reflected patterns can be tracked by optical flow tracking and motion point tracking.

4.1.6. Circular laser

Circular laser can provide rich welds geometry and position information. The principle of circular laser is the rotation axis can spin around the center of the lens. Meanwhile the laser spot passes through the scanning lens glued together by the positive lens and the retro type lens at an incident angle (Xu et al., 2008a). Xu et al. (2007a) developed a circular laser vision sensor to locate weld seam and realize seam tracking. The linear-array CCD camera can be replaced by the area-array CCD camera. A 3D recovery model of the weldment based on the projection rules of circular laser has been established.

Fig. 27 shows that an intersecting curve can be generated when the circular laser is projected onto the surface of the weldment. $P(X_L, Y_L, Z_L)$ is a point which is on the intersecting curve. And the coordinate of $P(X_L, Y_L, Z_L)$ is the coordinate in the laser cone coordinate system $\{L\}$, of which corresponding image point is $P'(x_{pixel}, y_{pixel})$ in the pixel coordinate system $\{pixel\}$. The coordinate value in the camera coordinate system $\{C\}$ is $P'(x_c, y_c)$. According to the spatial relation and imaging principle, the following equation can be obtained.

$$\begin{cases} X_L = -x_c \cos \beta + l \sin \beta \\ Y_L = -y_c \\ Z_L = l \cos \beta + x_c \sin \beta \end{cases} \quad (19)$$

Where, l is the distance between the original point in the camera coordinate system $\{C\}$ and the original point in the laser cone coordinate system $\{L\}$. β is the angle between the axis of the diode laser and the light axis of the CCD camera.

Advanced gradient method and 3×3 mask method are used to locate the weld seam of the lap joint. Fig. 28 (a) illustrates the orig-

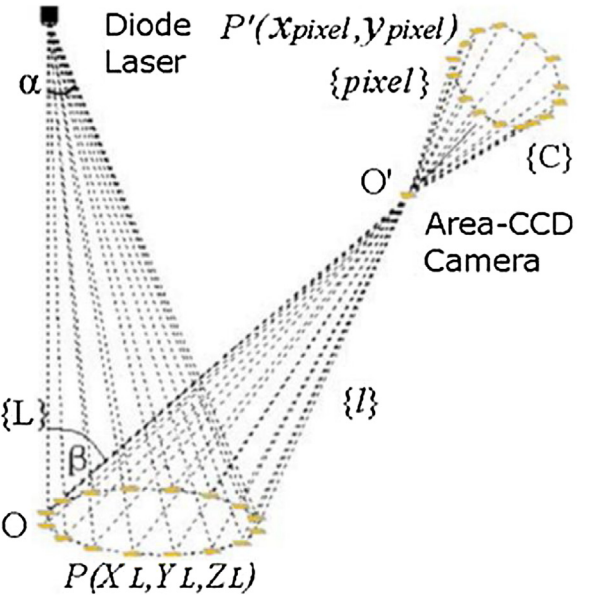


Fig. 27. The 3D recovery model based on circular laser projection rules (Xu et al., 2007a, a).

inal image and Fig. 28 (b) shows the result of image segmentation. In order to simplify the location process, the mask method is proposed. The mask method used in weld seam location depends on two related factors: the spatial extent of the mask and the number of pixels involved in the median computation. For the lap joint location, a 3×3 mask is put forward with high efficiency and processing velocity. Fig. 28 (c) shows the 3×3 mask. Every element in 3×3 mask is computed with the grayscale value of lap joint A, B, C and

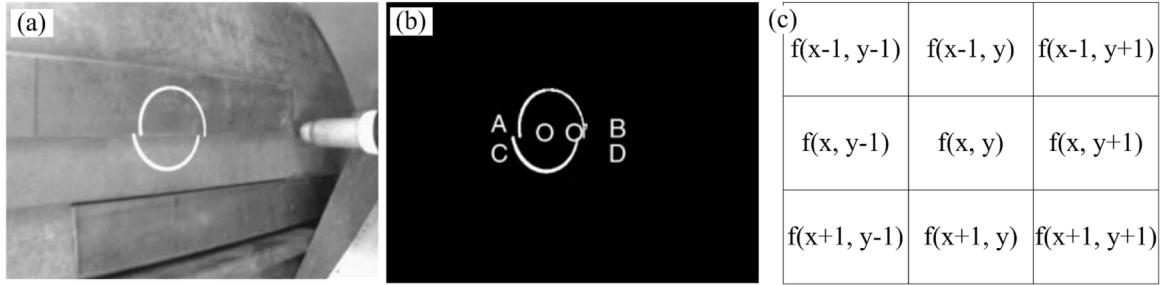


Fig. 28. The weld seam was located by a circular laser in a lap joint: (a) original image, (b) image segmentation, (c) 3×3 mask (Xu et al., 2007a).

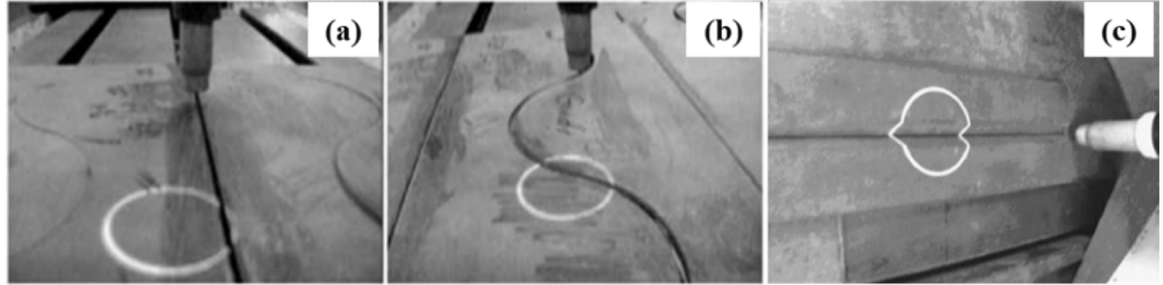


Fig. 29. Weld seam tracking based on circular laser vision sensor: (a) I-type butt joint, (b) sine-type butt joint, (c) V-type butt joint (Xu et al., 2007a,Xu et al., 2007b).

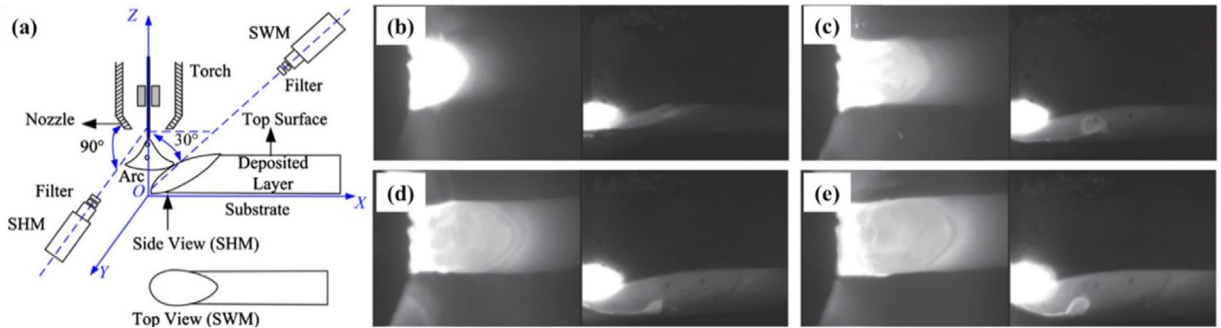


Fig. 30. The welding layer width and height of various layers in GMAW: (a) the measure principle, (b), (c), (d) and (e) the first, second, third and fourth layer (Xiong and Zhang, 2013).

D, respectively. The experimental and theoretical 3D coordinates of position A, B, C and D can be calculated by this paper.

Xu et al. (2007b) also realized weld seam tracking of I-type, sine-type and V-type (Xu et al., 2008b) butt joint by adapting circular laser vision sensor. As shown in Fig. 29. The relationship between the depth information of weldment and the off-axis angle can be investigated. And weld seam tracking experiments can be carried out. The main errors of this system are analyzed, including the calibration error and the light scanning error.

Six typical laser structured lights assisted vision sensor can be called laser vision sensor. Generally, laser vision sensor mainly consists of diode laser, filter and image acquire device CCD or CMOS (complementary metal-oxide semiconductor) (Rout et al., 2019). Correspondingly, laser sensor mainly consists of laser, laser detector and measuring circuit (Laser sensor, 2020). The differences of the two sensors are the composition structure and detection principle. Their composition structures have been described, respectively. The detection principle of laser vision sensor is that the laser diode may produce a stripe or other graphs which would be captured by the camera. The feature information can be extracted by built-in algorithm. The detection principle of laser sensor is laser triangulation method or laser pulse echo analysis method (Zha and Li, 2015).

There is a little difference between laser stripe and laser structured light. Laser stripe generally is generated by the line laser, such as single-line laser, cross-lines laser, multi-lines laser. Therefore, laser stripe includes single laser stripe, two laser stripes, three laser stripes etc. Laser structured light not only includes the light projected by the line laser, but also included circular laser and dot matrix laser. The graph generated by circular and dot matrix laser are not laser stripe. Therefore, the range of laser structured light is larger than that of laser stripe.

4.2. Passive vision sensing

Compared with active vision sensing, passive vision sensing has the advantages of good real-time, simple installation, better accessibility (Stansfield, 1988). Especially, there is no look-ahead detection and unique feature information can be obtained during welding. The passive vision method directly utilizes the ambient or arc light as the background light source.

4.2.1. Welding layer measurement

Xiong et al. (Xiong and Zhang, 2013) utilized two passive vision sensors with a neural and a narrow-band filter to online measure the welding layer width and height, respectively, in wire and arc

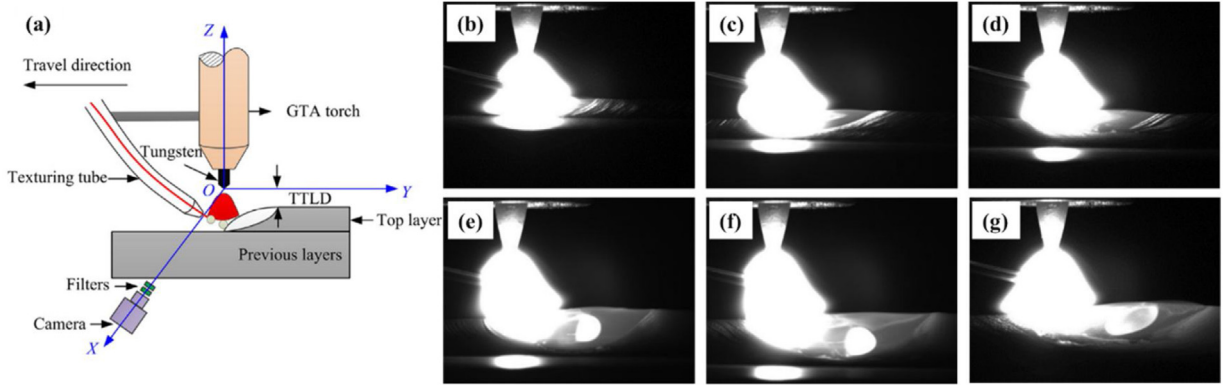


Fig. 31. The welding layer height of various layers in GTAW: (a) the measure principle, (b), (c), (d), (e), (f) and (g) the first, second, third, fourth, fifth and sixth layer (Xiong et al., 2019).

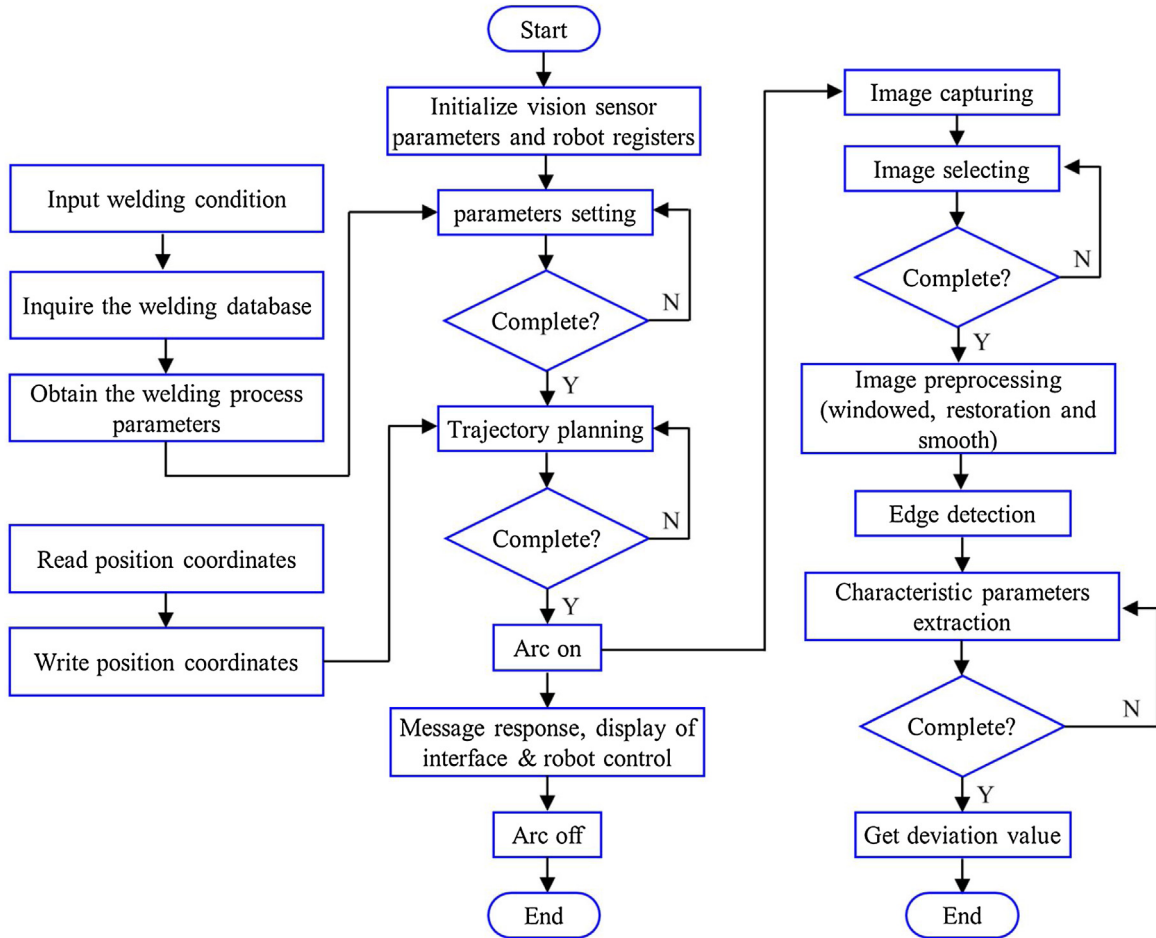


Fig. 32. The flowchart of weld seam tracking procedures for robotic GTAW and GMAW (Xu et al., 2015).

additive welding. The radiation lights from the arc of GMAW can be regarded as the light source. As shown in Fig. 30. They (Xiong et al., 2019) also realized automatic determination of welding layer height in robotic GTAW by calculating the TTLD (tungsten to top layer distance). As shown in Fig. 31. The detection precision can be verified by the experiments and the detection error of the TTLD is less than 3 %.

4.2.2. Weld pool detection

The weld pool morphology is not only related to the welding process, but also considered as the detection object (Lei et al., 2018).

Xu et al. (2012) used the purpose-designed passive vision system to acquire the clear weld images, including the weld pool and the weld center. The morphological parameters of the weld images can be extracted by a new improved canny algorithm. The precision of the image processing approach in GTAW and GMAW can be controlled within ± 0.17 mm and ± 0.3 mm, respectively (Xu et al., 2015). Fig. 32 shows the flowchart of weld seam tracking procedures for robotic GTAW and GMAW. In view of the fore-guiding error of active vision sensing, Gao et al. (2011) adopted passive vision sensing. The centroid characteristics of weld-pool images can be analyzed by passive vision system. The position, the displace-

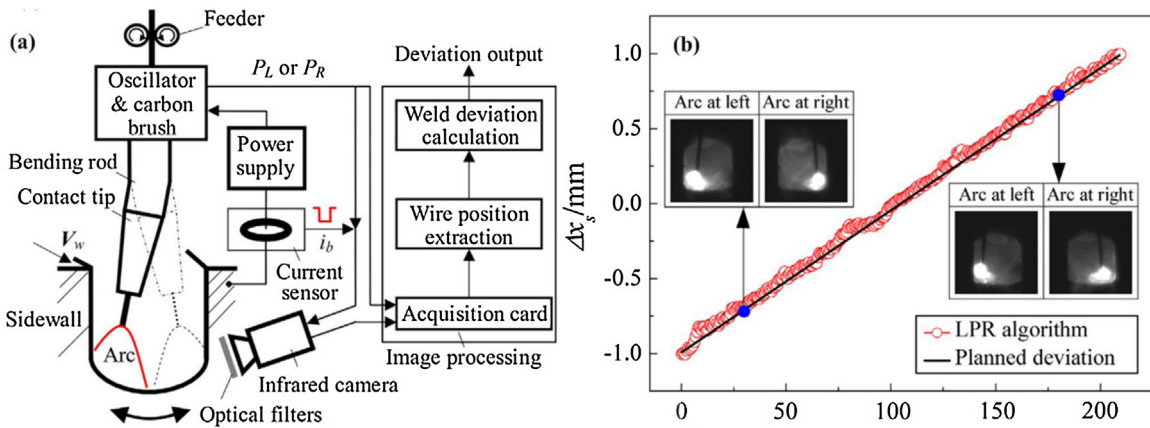


Fig. 33. The extraction of swing arc is used to detect the weld deviation in narrow gap: (a) the system setup, (b) The weld deviation detection results by LPR algorithm (Zhu et al., 2017).

ment and the moving velocity of the centroid can be regarded as the multiple input variables of a designed neural network model. The neural network vision model can be validated by the experiment.

4.2.3. Swing arc extraction

Li et al. (2015a) provided an improved feature extraction algorithm for swing arc image in narrow gap MAG (metal gas welding). The arc images can be captured by an infrared CCD camera. The images that belonged to the “left arc” group can be used to extract the right groove edge position. On the contrary, the images that belonged to the “right arc” group can be used to extract the left groove edge position. Zhu et al. (2017) developed a weld deviation detection system based on infrared vision sensing for swing arc narrow gap GMAW. When the swing arc stay at left or right groove sidewall, the arc images can be captured at the base period of pulsed current. The weld deviation feature can be extracted from the relative distance from the electrode wire center to the opposite sidewall. The LPR (local pattern recognition) algorithm in searching the trust position of groove edge can control the detection error within ± 0.086 mm. As shown in Fig. 33.

Although active vision sensing and passive vision sensing have a widely use in robotic welding, they can't cover the detection requirement in all welding situations. For example, a single CCD camera is hard to realize 3D weld seam tracking. This is because the weld depth information can't be detected by monocular vision. Structure light aided vision or binocular vision (Liu and Xu, 2018) can detect the weld depth information, however, their detection positions are in front of the welding position and their detection accuracy are greatly influenced by the welding light. Passive vision sensing is not suitable for complex weld seam tracking. Therefore, in complex welding situations, vision sensing can be combined with arc voltage sensing, acoustic sensing and temperature sensing etc. In collaboration with other sensors, the ability of weld seam tracking can be greatly improved (You et al., 2014). This is multiple sensors fusion.

Table 3 shows the common methods of vision sensing. Single-line laser owns many suitable image processing algorithms due to its widely use. However, not enough weld seam information can be detected. Cross-lines laser can detect the 2D information of the weld seam. Especially, it is suitable for T-shaped and Cross-shaped seams etc. But there are special requirements for the installation of cross-lines laser. Multi-lines laser can be adaptable to space curve and other complex weld seams. However, the corresponding algorithm is complicated. Grid lines laser can detect the finished and the next weld seams for multi-layer and multi-pass welding. The main issue of this method is large computation and high require-

ment for laser source. The advantages of dot matrix laser are wide coverage and high sensitivity, which can realize real-time measurement of a 3D weld pool surface. The disadvantages are also obvious. It is just suitable for some specific welding situations. Circular laser can provide rich geometric and positional information of weld seam. However, the algorithm needs to be customized. Passive vision sensing is not as widely used as active vision sensing in robotic welding. This is because this sensing method is usually suitable for straight line weld seam and owns high requirement for hardware configuration and process parameters. However, it has a unique merit so that it can't be replaced by active vision sensing. For example, welding layer and swing arc are hardly detected by active vision sensing.

5. Compensation and control

The purpose of compensation and control is to realize trajectory tracking. The continuous calculation of weld deviation information between the current point and the reference point is necessary for trajectory tracking. When the weld deviation signal can be obtained by the controller, several control strategies such as PID control Shen et al. (2010), fuzzy control (Fan et al., 2019c) and iterative learning control (Li et al., 2019) etc. can be adopted to rectify the position of welding torch to the correct weld position. Compensation and control usually can be divided into weld path detection, seam tracking algorithm and robot control strategy.

5.1. Weld path detection

Weld path detection usually includes three situations: (1) the detection point is ahead of the welding point (de Graaf et al., 2010), (2) the detection point is the same as the welding point (Xu et al., 2017), (3) the weld path is generated directly (Zhang et al., 2019). Generally, active vision sensing and laser displacement sensor are adopted in the first situation. This is because laser structured light is usually used to pre-detect the welds. Passive vision sensing and infrared vision sensing can be utilized in the second situation. This is because the weld pool and swing arc are taken as the detect object. The detection position coincides with the welding position. Off-line programming and active vision sensing can be used to the third situation. The detection of weld path is the foundation for robot compensation and control.

5.1.1. Front distance detection

Düzçükoğlu et al. (2018) adopts a laser distance sensor to detect the weld position in advance. There is a prediction interval between

Table 3

The common methods of vision sensing.

Vision sensing	Authors	Detection object	Application	Method	Merits	Demerits
• Single-line laser	• Fan et al. (2017)	• Symmetric V-groove, left and right sides V-groove, I-groove, left and right lap joints	• Different weld types can be recognized	• Feature vector computation method and SVM-based modeling method	• Many suitable image processing algorithms	• Not enough weld information is detected
Active vision sensing	• Lü et al. (Lü et al., 2018)	• I-groove and Y-groove weld	• The speed and accuracy of weld identification are improved	• Ridge line tracking method and direction template method		
	• Reichert et al. (Reichert and Peterson, 2007)	• Spot weld fractures	• The weld and electrodes of resistance spot welding are measured	• Laser vision is combined with optical geometry		
• Cross-lines laser	• Lei et al. (2020b)	• Tubesheet	• The welding height variation value can be detected	• Regional center extraction and least-square fitting	• Suitable for T-shaped and Cross-shaped seams etc.	• There are special requirements for the installation of cross-lines laser
	• Zhang et al. (2014a)	• The horizontal and vertical weld lines	• Weld line detection and tracking	• Spatial-temporal cascaded hidden Markov models		
	• Li et al. (2010)	• Aperture	• Aperture detection and visual alignment	• Intensity mapping and features extraction		
• Multi-lines laser	• Zhang et al. (2018a)	• T-joint	• Weld seam tracking	• Piecewise fitting and Freeman chain code marking method	• Adaptable to space curve and other complex weld seams	• The algorithm is complicated
	• Zou et al. (Zou et al., 2018a)	• Butt seam, lap seam and complex curve seam	• Weld seam tracking	• Weld feature detection algorithm is based on kernelized correlation filter		

Table 3 (Continued)

Vision sensing	Authors	Detection object	Application	Method	Merits	Demerits
Passive vision sensing	• Guo et al. (2019)	• Weld groove with different joint types	• The cross-sectional size of weld groove and welding torch height can be measured	• The detection algorithm is derived from optical triangulation		
	• Zhang et al. (2017)	• Big V-groove	• Multi-layer and multi-pass welding	• The grid intersection extraction algorithm	• The finished and the next weld seams can be detected	• Large computation and high requirement for laser source
	• Jia et al. (2019)	• Weld surface	• 3D construction of weld	• Laser-photo hybrid method		
	• Zhang et al. (2013) and Saeed et al. (2004)	• Weld pool surface	• Real-time measurement of a 3D weld pool surface	• Reconstruction algorithm is based on the slope field of the reflected laser pattern	• Wide coverage and high sensitivity	• Just suitable for some specific welding situations
	• Xu et al. (2007b), b	• I-groove and V-groove straight line weld, I-groove sine-shaped weld	• Weld seam tracking	• Image processing model and 3D calculation algorithm	• Providing rich geometric and positional information	• The algorithm needs to be customized
	• Welding layer measure	• Welding layer	• The measurement of the welding layer geometry	• Image processing algorithm is based on characteristic points	• The welding layer width and height are measured	• The vision system is complex
	• Xu et al. (2015), 2012	• Weld pool and seam	• Weld seam tracking	• A new improved edge detection algorithm	• Real-time tracking can be realized	• Susceptible to process parameters
	• Gao et al. (2011)	• Weld pool	• Weld seam tracking	• Neural network vision model		
	• Li et al. (2015a)	• Arc and groove	• Weld seam tracking and penetration control in swing arc narrow gap welding	• A modified weld image feature extraction algorithm	• Adaptable to large groove depth	• Infrared CCD camera is required
	• Zhu et al. (2017)	• Arc and groove	• Weld deviation detection	• Local pattern recognition algorithm		

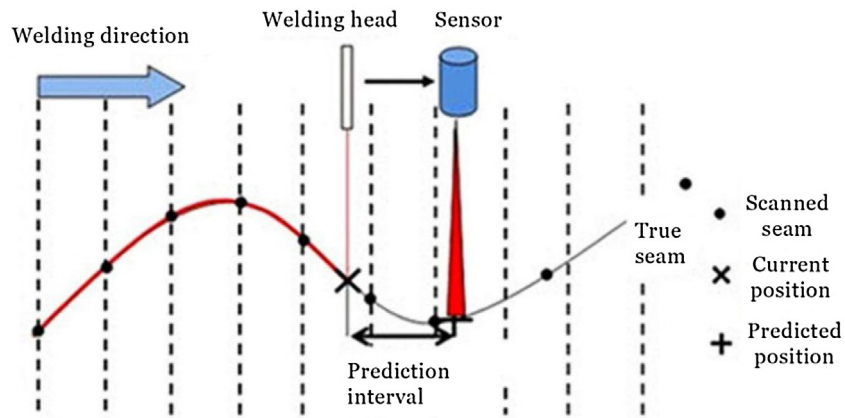


Fig. 34. The system delay prediction model (Düzcükoğlu et al., 2018).

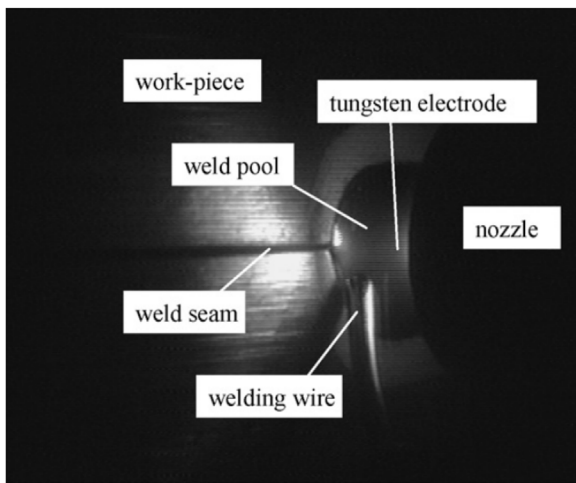


Fig. 35. The welding image (Xu et al., 2012).

the sensor and the welding head. The sensor pre-scans the weld seam and calculate the prediction position, which will guide for the current position. The system delay prediction model is illustrated in Fig. 34. Micallef et al. (2011) introduces a method to determine the weld shape and the start and end points of straight and curved seams. A brass pointer is used to simulate the weld path of welding wire with a camera paraxial installation on the termination of a robot. Guo et al. (2019) projects single-line & cross-lines laser structured lights in front of welding torch along the welding direction. The cross-section size of groove and the height of welding torch can be detected.

5.1.2. Current position detection

Xu et al. (2012) developed a passive vision system to acquire the welding image, shown in Fig. 35. The edges of seam and pool can be extracted by a new improved Canny algorithm. The welding position can be regarded as the detection position. Real-time seam tracking can be realized. Gao et al. (2011) adopted passive vision system to analyze the centroid characteristics of weld-pool images considering the fore-guiding error of active vision sensing. Zhu et al. (2017) developed a swing arc weld deviation detection system based on infrared vision sensing for narrow gap seam tracking. Daeinabi et al. (Daeinabi and Teshnehab, 2006) took weld path image every half cycle of weaving motion by a camera. The weld path information can be calculated by a computer after image process.

5.1.3. The generation of weld path

From Fig. 36 (a) we can see there are two CCD cameras in the robotic welding system. The installation mode of CCD camera 1 belongs to eye-in-hand. The installation mode of CCD camera 2 belongs to eye-to-hand. Jin et al. (2017) adopted CCD camera 1 to capture the whole image of a tubesheet. The detection path of CCD camera 2 can be obtained by an automatic route planning algorithm. The actual welding path of each tube can be obtained through the tube extraction and welding path planning. Ryberg et al. (2010) used a stereo vision algorithm and a novel camera model to determine the 3D geometry of weld joint. The off-line programming weld path can be corrected and updated. Tsai et al. (2011) developed a 3D machine vision technique to recognize the weld seam and generate a weld path for the golf-club head. Dinhamb et al. (Dinhamb and Fang, 2013) realized the identification and localization of the saw-tooth seam and curve weld by computer stereo vision. The fillet weld joints of any shape without prior knowledge can also be detected (Dinhamb and Fang, 2014). The adopted method in the captured image is adaptive line growing algorithm.

Table 4 shows the comparisons of weld path detection methods. Front distance detection, current position detection and the generation of weld path are the common methods in weld path detection. Front distance detection is available to many types of weld seams. And active vision sensing usually takes this approach. However, a delay model should be taken into consideration. The advantage of current position detection is good real-time in seam tracking. Passive vision sensing usually adopts this method. However, the depth of weld seam is difficult to detect. The generation of weld path is easy to control the motion of welding torch. However, it can't perceive the state of the weldment. And off-line programming usually takes this method.

5.2. Seam tracking algorithm

Although the weld path can be generated, the actual welding path maybe varied due to the factors such as thermal deformation, detection error and positioning error etc. Therefore, it is essential to realize real-time weld seam tracking in robotic welding (Zeng et al., 2017). Meantime, it is an important issue to choose or design suitable algorithm to describe the weld deviation information. And the establishment of the tracking model is also a solution. The previous section has illustrated the weld path detection. This part will discuss the acquisition of deviation signal and the design of seam tracking algorithm.

Xu et al. (2017) extracted the deviation signal between the center point of weld pool and the centerline of seam. Then the incremental interpolation algorithm can be used to adjust the robot

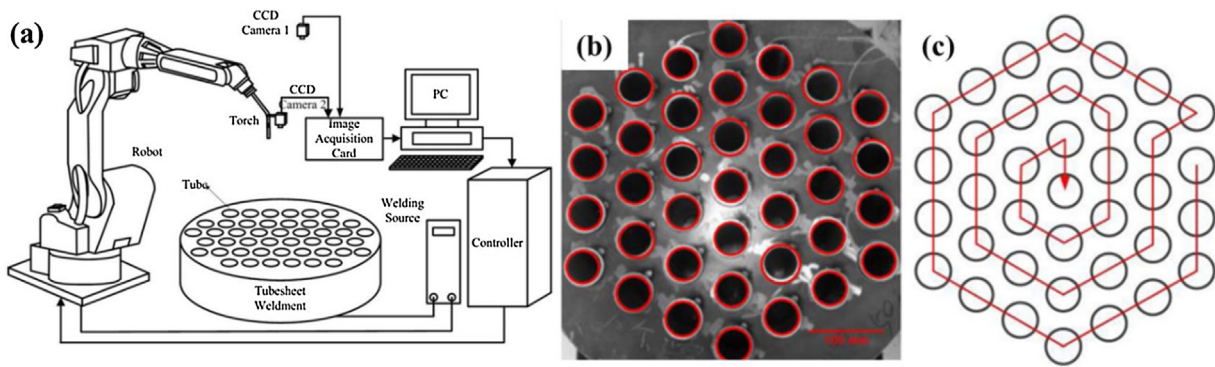


Fig. 36. Automatic tube-to-tubesheet welding: (a) the system setup, (b) tube extraction, (c) welding path planning (Jin et al., 2017).

Table 4

The common methods of weld path detection.

Detection methods	Authors	Merits	Demerits	
Weld path detection	<ul style="list-style-type: none"> Front distance detection Current position detection The generation of weld path 	<ul style="list-style-type: none"> Düzcükoğlu et al. (2018); Micallef et al. (2011) Xu et al. (2012); Zhu et al. (2017) Jin et al. (2017); Tsai et al. (2011) 	<ul style="list-style-type: none"> Available to many types of weld seams Good real-time in seam tracking The motion of welding torch is easy to control 	<ul style="list-style-type: none"> A delay model should be taken into consideration The depth of weld is difficult to detect It can't perceive the state of the weldment

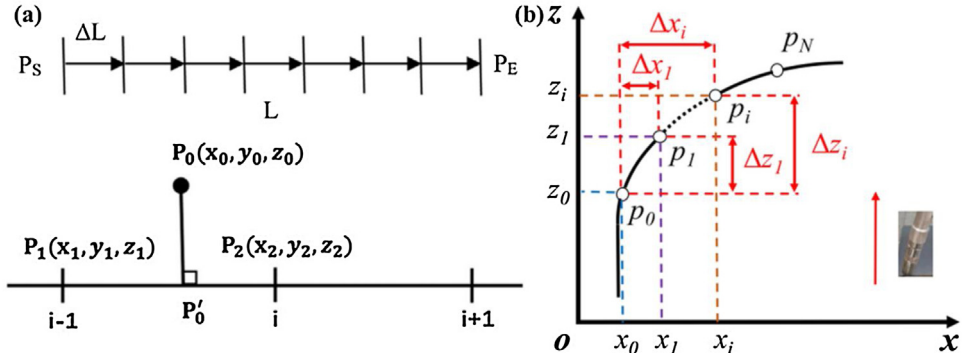


Fig. 37. Seam tracking algorithm: (a) incremental interpolation algorithm, (b) absolute interpolation algorithm (Lei et al., 2020a; Xu et al., 2017).

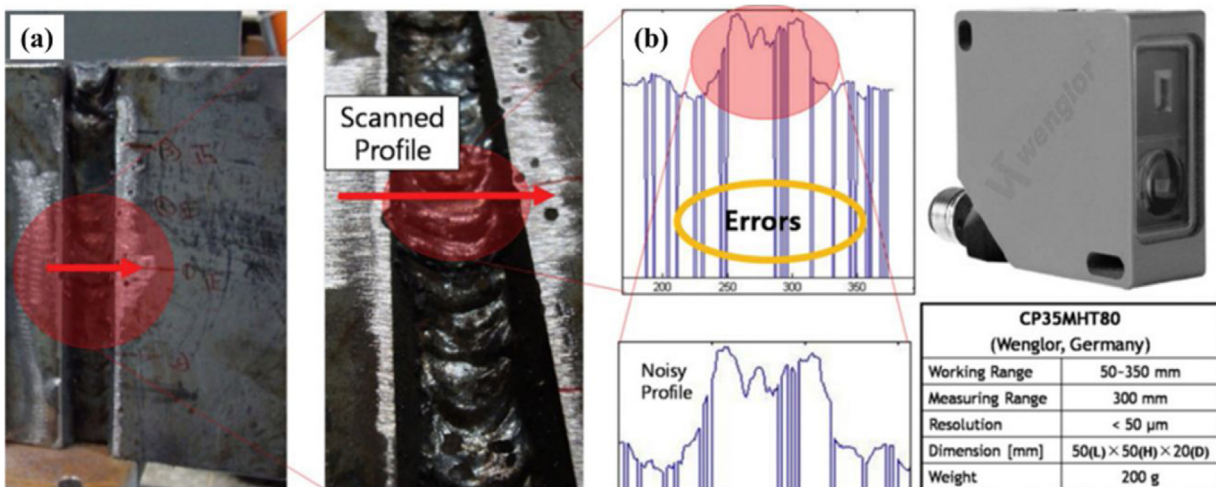


Fig. 38. A differential characteristic-point detection algorithm: (a) single-V butt multi-pass weld, (b) laser displacement sensor (Chang et al., 2012).

Table 5

The common methods of weld seam tracking.

Authors	Weld seam trajectory	Weld joints	Tracking algorithm/method	Merits	Demerits
Kiddee et al. (2016)		• Butt joint	• Adapted line fitting algorithm	• Huge computational cost can be reduced	• The detection result is sensitive to the lighting conditions
Wu et al. (2015)	• Straight line weld		• Feature points detection and centerline extraction	• Less computing time and less occupying memory	• The threshold of binarization needs statistical evaluations
Shah et al. (2017)			• Shape algorithm between start, mid, auxiliary and end points	• Suitable for various weld paths	• Auxiliary points are necessary
Xue et al. (2019)			• Kalman filter iterated algorithm	• The 3D position of the butt joint can be detected	• The width of the butt joint is less than 0.2 mm
Gao et al. (2017)			• Optical flow and particle filter algorithm	• The average tracking error can be reduced to 0.01 mm	• The welding system is a bit complicated
Li et al. (2017)		• Fillet joint	• Double-threshold recursive least square method	• Improving the real-time performance and accuracy	• Requiring slightly more computational time
Xu et al. (2017)			• Incremental interpolation algorithm	• It can be used for passive vision sensing	• The robot's trajectory is interpolated with 3–5 mm
Xu et al. (2007a)		• Lap joint	• Circle-depth relation algorithm	• The 3D information of the weld seam can be calculated	• The detection accuracy needs to be improved
Zou et al. (2018a)		• Butt joint	• Kernelized correlation filter algorithm	• Determining the location of the weld feature quickly and accurately	• Sample training and classification testing are necessary
Shah et al. (2017)	• Plane curve weld		• Shape algorithm between start, mid, auxiliary and end points	• Suitable for various weld paths	• Auxiliary points are necessary
Bae et al. (2002)			• Symmetric algorithm of the weld pool around the wire	• The weld seam tracking of steel pipe root pass is realized	• The maximum correction data for the weld seam are limited to 0.5 mm
Ding et al. (2016)			• Shape-matching algorithm	• It can be used for seam tracking in various groove types	• The interval of the two adjacent laser stripes in Z-direction is 0.25 mm
Zou et al. (2018a)		• Lap joint	• Kernelized correlation filter algorithm	• The location of the weld feature can be determined quickly and accurately	• Sample training and classification testing are necessary
Wei et al. (2011)		• Butt joint	• Position error extraction algorithm	• It can be used for passive vision sensing	• The detection accuracy needs to be improved
Lei et al. (2020a)	• Space curve weld		• Absolute interpolation algorithm	• Robust and stable	• The front distance is a bit larger
Xue et al. (2019)			• Kalman filter iterated algorithm	• The 3D position of the butt joint can be detected	• The width of the butt joint is less than 0.2 mm
Zhang et al. (2019)		• Lap joint	• Cubic smoothing spline fitting	• Stronger anti-interference capability and higher curve smoothness	• The 3D point cloud data is necessary

trajectory in real-time, shown in Fig. 37 (a). Lei et al. (2020a) obtained the right-left deviation and up-down offset of the weld path by two contact-type sensors. The position coordinates of the detection point in weld groove can be calculated by absolute interpolation algorithm. The original point is regarded as the reference point, shown in Fig. 37 (b). Chang et al. (2012) developed a differential characteristic-point detection algorithm for single-V butt multi-pass weld using a laser displacement sensor, shown in Fig. 38.

The cross-section of the seam profile can be scanned by the sensor and the noise can be removed by Gaussian filter.

Bae et al. (2002) pointed that the shadow of the wire indicated the current position of the welding torch and the center of weld pool represented the groove center. The idea of seam tracking is to sustain a symmetry of the weld pool around the wire. Xue et al. (2019) even smoothed the detection results of position and orientation sent to the robot, in order to eliminate the dithering of robot

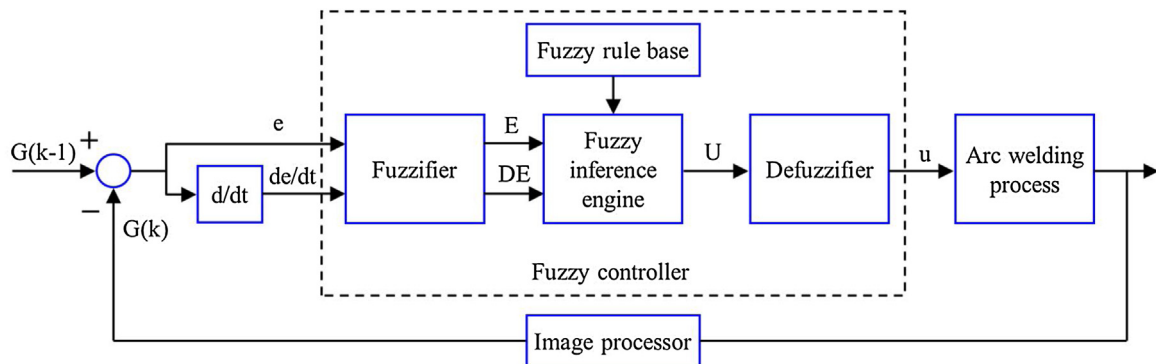


Fig. 39. The diagram of fuzzy controller (Bae et al., 2002).

motion. The results show that Kalman filter iterated algorithm is quite applicable for the robotic seam tracking. The common methods of weld seam tracking are shown in Table 5. The merits and demerits of these seam tracking algorithms are listed. The important issue of seam tracking is to choose or design suitable algorithm to describe the weld deviation information. And the establishment of the tracking model is also a solution.

5.3. Robot control strategy

Generally, there are two common methods to select the reference value. The first method is to regard the initial value as the reference value. The error is the difference between the initial value and the controlled variable. The second method is to regard the previous value as the reference value. Then the error is the difference between the previous value and the controlled variable. Bae et al. (2002) designed a fuzzy logic controller to understand the relation between gap size and welding conditions. The measured gap size can be used to determine the appropriate welding conditions. The gap value $G(k-1)$ of the previous moment is regarded as the reference value. The current value $G(k)$ is the controlled variable. As shown in Fig. 39, Zou et al. (2018b) applied PD (proportional-derivative) control in laser vision seam tracking system. The advantage of PD control is that the response time to the control signals is fast. Huang et al. (Huang and Kovacevic, 2012) proposed a close-loop PID control method, which can compensate for the position error between the desired position and the actual position of the tracking point. Liu et al. (2014) adopted particle swarm algorithm to improve PID control of seam tracking. Zou et al. (2018a) realized an adaptive fuzzy control method in a 3-lines laser vision seam tracking control system.

Ma et al. (2010) studied a control model between the rectifying voltage and the offset (between the torch and the seam center). Based on this model, the fuzzy PID controller can be designed for all kinds of offsets. Graaf et al. (de Graaf et al., 2010) even adopted a trajectory-based control method to track straight and curved trajectories. They presented 4 major advantages than the common control approaches based on time. Li et al. (2019) considered the extremely variable of welding environment and the jumping change in parameters. The idea of multiple model adaptive control can be introduced into iterative learning control.

Table 6 shows the common control methods in robotic welding. The selection of control method is determined by weld path detection and seam tracking algorithm. This is because detection position and deviation calculation are determined by weld path detection and seam tracking algorithm, respectively. These parameters are generally regarded as the input of control methods.

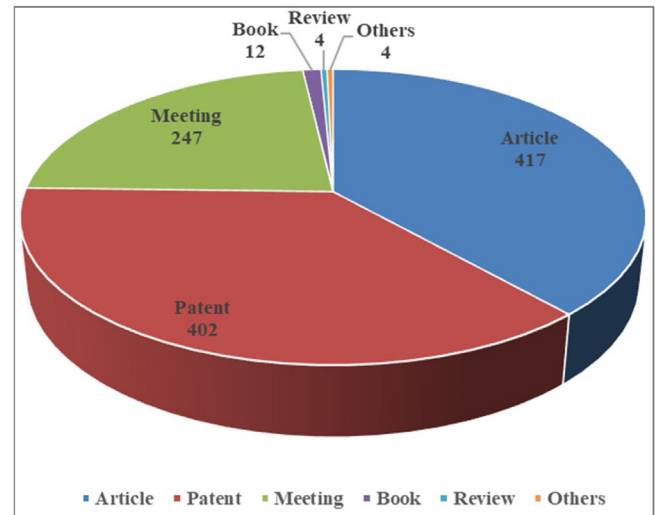


Fig. 40. The literatures involved with the topics.

6. Review process

This paper reviews the whole procedures and covers all aspects of the vision-aided robotic welding. Through retrieval and analysis in Web of Science (topic: robot welding and vision, timespan: 2000–2020), there are many literatures about these topics. The following picture shows the details. There are 417 articles, 402 patents, 247 meetings, 12 books, 12 reviews and 4 others on these topics (Fig. 40).

Furthermore, enter the topic vision sensor calibration, hand eye calibration, start welding point positioning, laser vision, passive vision, seam tracking and control method into the search box, separately. Use them to refine the first search results, respectively.

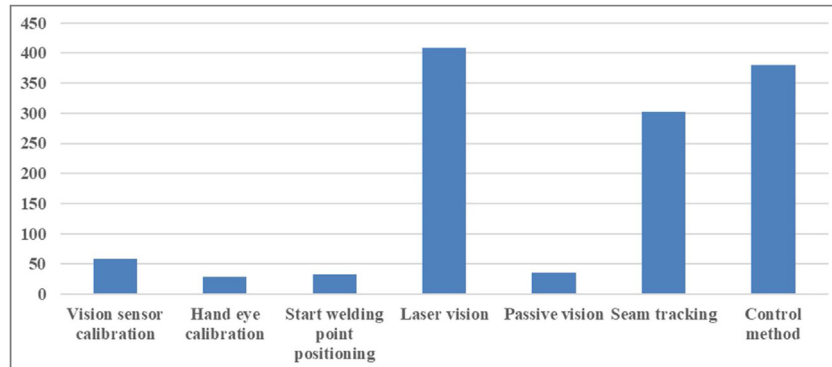
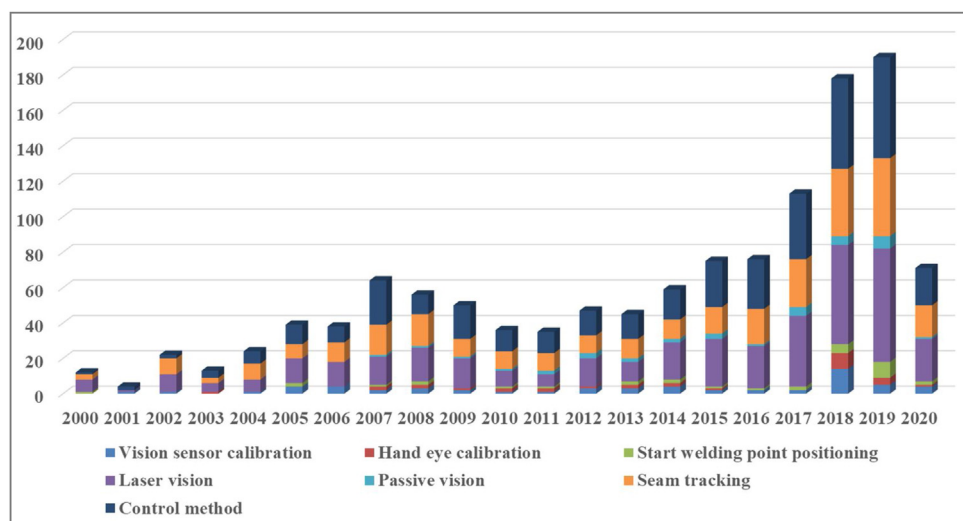
From 2000–2020, there are 59 records about vision sensor calibration, 30 records about hand eye calibration, 32 records about start welding point positioning, 409 records about laser vision, 35 records about passive vision, 302 records about seam tracking and 380 records about control method. The following picture Figure 41 shows the details (Fig. 41).

Fig. 42 shows the number of literatures in each section in every year from 2000 to 2020. It can be observed from the figure Figure 42 that laser vision (active vision) occupies the most literatures. The reason may be the accuracy and efficiency of laser vision are practical for robotic welding. Control method and seam tracking are the next most literatures. It means that in addition to vision sensing, control method and tracking algorithm are the two remaining research hotspots. In recent years, the literatures of vision-aided robotic welding show an obvious upward trend. The number of

Table 6

The common control methods in robotic welding.

Control method	Merits	Demerits
PD control (Kiddee et al., 2016; Zou et al., 2018b; Tomei, 1991)	<ul style="list-style-type: none"> Fast response and suitable for deviation control 	<ul style="list-style-type: none"> The control precision and stability need to be improved
PID control (Xu et al., 2012; Liu et al., 2014; Lv et al., 2014)	<ul style="list-style-type: none"> Wide use and better dynamic response 	<ul style="list-style-type: none"> Adjusting PID parameters is complicated
Fuzzy control (Wei et al., 2011; Zou et al., 2018a; Düzüköglü et al., 2018; Kim and Rhee, 2001)	<ul style="list-style-type: none"> An accurate mathematical model is not essential 	<ul style="list-style-type: none"> The control variables should be determined by multiple experiments
Fuzzy PID control (Ma et al., 2010; Fan et al., 2019c)	<ul style="list-style-type: none"> It can be designed for all kinds of offsets and fuzzy control can optimize PID parameter 	<ul style="list-style-type: none"> The control principle is complicated and fuzzy rule should be reasonable
ICL (iterative learning control) (Li et al., 2019; Zhao et al., 2015)	<ul style="list-style-type: none"> For repetitive systems, iterative learning control is an effective and high accuracy control method 	<ul style="list-style-type: none"> The model of ICL should be established and simulation analysis is necessary
Trajectory-based control (de Graaf et al., 2010)	<ul style="list-style-type: none"> Cartesian locations of welding torch are added to the robot trajectory and all locations can be filtered 	<ul style="list-style-type: none"> The tracking error of curve trajectory is large

**Fig. 41.** The total number of literatures in each section from 2000 to 2020.**Fig. 42.** The number of literatures in each section in every year from 2000 to 2020.

literatures in 2020 is relatively small. This is because this year's quantity will not be counted until 2021. Therefore, this review has a certain scientific value and practical significance.

7. Conclusions and future development

7.1. Conclusions

This paper illustrates the main development, procedures, principles and methods of vision-aided robotic welding. From the review analysis, the following content can be summarized:

- (1) A calibration object is essential for vision sensor calibration. The calibration results are usually calculated by the commercial software or self-designed algorithm. The merits and demerits of the three common calibrations for vision sensor are analyzed. Hand-eye calibration is to solve the matrix that describes the relationship between the termination coordinate system and the camera coordinate system. Meanwhile, external device assistance is essential. Structured light aided vision calibration and 2D laser sensor aided calibration are probable the future directions due to their high accuracy.
- (2) In terms of SWP positioning, visual guidance is superior than teach-playback. It owns the ability to perceive the welding state of the weldment and realize autonomous positioning. The recognition, calculation and guidance control are the basic stages of visual positioning for SWP. The 3D coordinates of SWP can be calculated by many image processing algorithms. Then, PID control is the common control method to realize positioning. Meanwhile, laser vision guidance occupies an important position in the visual guidance.
- (3) The application range of active vision sensing is larger than that of passive vision sensing. Active vision sensing usually takes laser structured light as auxiliary light source. Various groove types (I-groove, V-groove, Y-groove, U-groove etc.) and joint types (butt joint, lap joint, fillet joint etc.) can be detected by 6 typical active vision sensing methods. Passive vision sensing usually regards the ambient or arc light as the background light source. The width and height of welding layer, weld pool morphology and swing arc feature can be monitored by passive vision sensing.
- (4) Front distance detection is available to many types of weld seams. And active vision sensing usually takes this approach. However, a delay model should be taken into consideration. The advantage of current position detection is good real-time in seam tracking. Passive vision sensing usually adopts this method. However, the depth of weld seam is difficult to detect. The generation of weld path is easy to control the motion of welding torch. However, it can't perceive the state of the weldment. And off-line programming usually takes this method.
- (5) Seam tracking algorithms and control methods have also been introduced in detail. The important issue of seam tracking is to choose or design suitable algorithm to describe the weld deviation information. And the establishment of the tracking model is also a solution. Various weld seam trajectories (straight line, spatial, zig-zag, sine, half-moon, pipe curve etc.) can be compensated by several common control methods (PID control, fuzzy control, iterative learning control, trajectory-based control etc.). The selection of control method is determined by weld path detection and seam tracking algorithm.

7.2. The future development

The future development of vision-aided robotic welding is to avoid teach-playback. And more advanced technology can be

adopted to realize weld seam location and tracking. The following illustration maybe the future research direction.

- (1) **3D point cloud technology:** The robotic field is aware of the development of 3D object modeling technology. And research based on 3D point cloud data has led to new object recognition. Many of the available approaches for object recognition are grouped in standard vision packages, such as HALCON based on 2D data, Point Cloud Library based on 3D data (.). The 3D point cloud technology can fulfill the 3D reconstruction of working environment and localization of weld joint (Zhang et al., 2018b). The workpiece and the initial welding position can be identified.
- (2) **SLAM (simultaneous localization and mapping):** It is a mature technology in AGV (automated guided vehicle) field. However, it has not been used in robotic welding. The 2D or 3D working environment map of robotic welding can be built. The approximate coordinates of welding position for welding robot can be calculated by SLAM. The positioning accuracy maybe in centimeter scale according to the performance of AGV in warehouse. After the robot is positioned near the welding position by SLAM technology, the vision sensing can provide the robot with accurate coordinates of welding position.

Funding

This research is supported by China Postdoctoral Science Foundation (2018M632832), National Natural Science Foundation of China (51905191), National Natural Science Foundation of China (51805190), National Natural Science Foundation of China (51721092), Major Project of Science Research of Hubei Province (2018AAA027), Wuhan Science and Technology Planning Project (201903070311520), Launch Fund of Huazhong University of Science and Technology (05), Hubei Provincial Education Department Scientific Research Plan Guiding Project (B2019246).

Availability of data and material

Not applicable.

Code availability

Not applicable.

Authors' contributions

Ting Lei drafts the work and revises it critically for important intellectual content. Youmin Rong makes substantial contributions to the conception or design of the work. Hui Wang collects the references and figures. Min Li polishes up the language. Yu Huang approves the final version.

Declaration of Competing Interest

The authors report no declarations of interest.

References

- Bae, K.Y., Lee, T.H., Ahn, K.C., 2002. An optical sensing system for seam tracking and weld pool control in gas metal arc welding of steel pipe. *J. Mater. Process. Technol.* 120, 458–465.
- Bouguet, J., 2008. Camera Calibration Toolbox for Matlab, CaltechUniversity. http://www.vision.caltech.edu/bouguetj/calib_doc/.
- Chang, D., Son, D., Lee, J., Lee, D., Kim, T.W., Lee, K.Y., Kim, J., 2012. A new seam-tracking algorithm through characteristic-point detection for a portable welding robot. *Robot. Comput. Manuf.* 28, 1–13, <http://dx.doi.org/10.1016/j.rcim.2011.06.001>.

- Chen, X.Z., Chen, S.B., 2010. The autonomous detection and guiding of start welding position for arc welding robot. *Ind. Rob.* 37, 70–78, <http://dx.doi.org/10.1108/01439911011009975>.
- Chen, S.B., Lv, N., 2014. Research evolution on intelligentized technologies for arc welding process. *J. Manuf. Process.* 16, 109–122, <http://dx.doi.org/10.1016/j.jmapro.2013.07.002>.
- Chen, S.B., Chen, X.Z., Qiu, T., Li, J.Q., 2005. Acquisition of weld seam dimensional position information for arc welding robot based on vision computing. *J. Intell. Robot. Syst. Theory Appl.* 43, 77–97, <http://dx.doi.org/10.1007/s10846-005-2966-6>.
- Chen, X., Chen, S., Lin, T., Lei, Y., 2006. Practical method to locate the initial weld position using visual technology. *Int. J. Adv. Manuf. Technol.* 30, 663–668, <http://dx.doi.org/10.1007/s00170-005-0104-z>.
- Chen, S.B., Wang, W.Y., Ma, H.B., 2010. Intelligent control of arc welding dynamics during robotic welding process. *Mater. Sci. Forum.* 638–642, 3751–3756, <http://dx.doi.org/10.4028/www.scientific.net/MSF.638-642.3751>.
- Chen, H., Li, H., Gao, H., Wu, L., 2011. Kalman filtering for seam tracking in master-slave robot remote welding system. *Adv. Mater. Res.* 314–316, 1005–1008, <http://dx.doi.org/10.4028/www.scientific.net/AMR.314-316.1005>.
- Chen, H., Fang, Z., Xu, D., Sun, H., 2013. Vision based starting position recognition and positioning control for thin steel sheet welding robot. *Robot.* 35, 90–97, <http://dx.doi.org/10.3724/SP.J.1218.2013.00090>.
- Corke, P.I., 2007. A simple and systematic approach to assigning denavit–Hartenberg parameters. *IEEE Trans. Robot.* 23, 590–594, <http://dx.doi.org/10.1109/rr.2012.6180941>.
- Daeinabi, K., Teshnehlab, M., 2006. *Seam tracking of intelligent Arc welding robot. WSEAS Trans. Syst.* 5, 2600–2605.
- De, A., Parle, D., 2003. Real time seam tracking system for automated fusion arc welding. *Sci. Technol. Weld. Join.* 8, 340–346, <http://dx.doi.org/10.1179/136217103225005471>.
- Graaf, M.D., Aarts, R., Jonker, B., Meijer, J., 2010]. Real-time seam tracking for robotic laser welding using trajectory-based control. *Control Eng. Pract.* 18, 944–953, <http://dx.doi.org/10.1016/j.conengprac.2010.04.001>.
- Ding, Y., Huang, W., Kovacevic, R., 2016. An on-line shape-matching weld seam tracking system. *Robot. Comput. Manuf.* 42, 103–112, <http://dx.doi.org/10.1016/j.rcim.2016.05.012>.
- Dinham, M., Fang, G., 2009]. A low cost hand-eye calibration method for arc welding robots. In: 2009 IEEE International Conference on Robotics and Biomimetics, IEEE, pp. 1889–1893, <http://dx.doi.org/10.1109/ROBIO.2009.5420552>.
- Dinham, M., Fang, G., 2013. Autonomous weld seam identification and localisation using eye-in-hand stereo vision for robotic arc welding. *Robot. Comput. Manuf.* 29, 288–301, <http://dx.doi.org/10.1016/j.rcim.2013.01.004>.
- Dinham, M., Fang, G., 2014. Detection of fillet weld joints using an adaptive line growing algorithm for robotic arc welding. *Robot. Comput. Manuf.* 30, 229–243, <http://dx.doi.org/10.1016/j.rcim.2013.10.008>.
- Driels, M.R., Swazley, W., Potter, S., 1993. Full-pose calibration of a robot manipulator using a coordinate-measuring machine. *Int. J. Adv. Manuf. Technol.* 8, 34–41, <http://dx.doi.org/10.1007/BF01756635>.
- Du, R., Xu, Y., Hou, Z., Shu, J., Chen, S., 2019. Strong noise image processing for vision-based seam tracking in robotic gas metal arc welding. *Int. J. Adv. Manuf. Technol.* 101, 2135–2149, <http://dx.doi.org/10.1007/s00170-018-3115-2>.
- Düzcüoğlu, H., Aydoğdu, Ö., ÖzTÜRK, A., Akkuş, H., 2018. Design and manufacture of a new two axes welding seam tracking system using laser sensor fuzzy logic control. *Sigma J Eng Nat Sci.* 36, 33–48.
- Fan, J.F., Jing, F.S., Fang, Z.J., Liang, Z.Z., 2016]. A simple calibration method of structured light plane parameters for welding robots. In: Proceedings of the 35th Chinese Control Conference, IEEE, pp. 6127–6132, <http://dx.doi.org/10.1109/ChiCC.2016.7554318>.
- Fan, J., Jing, F., Fang, Z., Tan, M., 2017. Automatic recognition system of welding seam type based on SVM method. *Int. J. Adv. Manuf. Technol.* 92, 989–999, <http://dx.doi.org/10.1007/s00170-017-0202-8>.
- Fan, J., Jing, F., Yang, L., Teng, L., Tan, M., 2019a. A precise initial weld point guiding method of micro-gap weld based on structured light vision sensor. *IEEE Sens. J.* 19, 322–331, <http://dx.doi.org/10.1109/JSEN.2018.2876144>.
- Fan, J., Jing, F., Yang, L., Long, T., Tan, M., 2019b. An initial point alignment method of narrow weld using laser vision sensor. *Int. J. Adv. Manuf. Technol.* 102, 201–212, <http://dx.doi.org/10.1007/s00170-018-3184-2>.
- Fan, J., Jing, F., Yang, L., Long, T., Tan, M., 2019c. A precise seam tracking method for narrow butt seams based on structured light vision sensor. *Opt. Laser Technol.* 109, 616–626, <http://dx.doi.org/10.1016/j.optlastec.2018.08.047>.
- Fang, Z., Xu, D., Tan, M., 2013. Vision-based initial weld point positioning using the geometric relationship between two seams. *Int. J. Adv. Manuf. Technol.* 66, 1535–1543, <http://dx.doi.org/10.1007/s00170-012-4437-0>.
- Feng, X., Cao, M., Wang, H., Collier, M., 2008. The comparison of camera calibration methods based on structured-light measurement. *Proc. - 1st Int. Congr. Image Signal Process.*, 155–160, <http://dx.doi.org/10.1109/CISP.2008.163>.
- Gao, X., Ding, D., Bai, T., Katayama, S., 2011. Weld-pool image centroid algorithm for seam-tracking vision model in arc-welding process. *IET Image Process.* 5, 410, <http://dx.doi.org/10.1049/iet-ipr.2009.0231>.
- Gao, X., Mo, L., You, D., Li, Z., 2017. Tight butt joint weld detection based on optical flow and particle filtering of magneto-optical imaging. *Mech. Syst. Signal Process.* 96, 16–30, <http://dx.doi.org/10.1016/j.ymssp.2017.04.001>.
- Guo, J., Zhu, Z., Sun, B., Yu, Y., 2019. Principle of an innovative visual sensor based on combined laser structured lights and its experimental verification. *Opt. Laser Technol.* 111, 35–44, <http://dx.doi.org/10.1016/j.optlastec.2018.09.010>.
- He, T., Fan, Y., Xie, Y., Wu, Q., 2013. Positioning method for a visual guiding system in a laser welding machine. *Sixth Int. Symp. Precis. Mech. Meas.* 8916, 89162A, <http://dx.doi.org/10.1117/12.2035699>.
- Huang, W., Kovacevic, R., 2012. Development of a real-time laser-based machine vision system to monitor and control welding processes. *Int. J. Adv. Manuf. Technol.* 63, 235–248, <http://dx.doi.org/10.1007/s00170-012-3902-0>.
- Iakovou, D., Aarts, R., Meijer, J., 2005. Sensor integration for robotic laser welding processes. *J. Chem. Inf. Model.* 53, 1689–1699, <http://dx.doi.org/10.1017/CBO9781107415324.004>.
- Jia, N., Li, Z., Ren, J., Wang, Y., Yang, L., 2019. A 3D reconstruction method based on grid laser and gray scale photo for visual inspection of welds. *Opt. Laser Technol.* 119, 105648, <http://dx.doi.org/10.1016/j.optlastec.2019.105648>.
- Jin, Z., Li, H., Zhang, C., Wang, Q., Gao, H., 2017. Online welding path detection in automatic tube-to-tubesheet welding using passive vision. *Int. J. Adv. Manuf. Technol.* 90, 3075–3084, <http://dx.doi.org/10.1007/s00170-016-9649-2>.
- Kiddee, P., Fang, Z., Tan, M., 2016. An automated weld seam tracking system for thick plate using cross mark structured light. *Int. J. Adv. Manuf. Technol.* 87, 3589–3603, <http://dx.doi.org/10.1007/s00170-016-8729-7>.
- Kim, C.H., Ahn, D.C., 2012. Coaxial monitoring of keyhole during Yb:YAG laser welding. *Opt. Laser Technol.* 44, 1874–1880, <http://dx.doi.org/10.1016/j.optlastec.2012.02.025>.
- Kim, Y., Rhee, S., 2001. Development of an arc sensor model using a fuzzy controller in gas metal arc welding. *Meas. Sci. Technol.* 12, 534–541, <http://dx.doi.org/10.1088/0957-0233/12/4/320>.
- Kochan, A., 2000. Automating the construction of railway carriages. *Ind. Robot An Int.* 27, 108–110, <http://dx.doi.org/10.1108/01439910010315427>.
- Kovacevic, R., Zhang, Yuming, 1996. Sensing free surface of arc weld pool using specular reflection: principle and analysis. *Proc. Inst. Mech. Eng. Part B J. Eng. Manuf.* 553–564.
- Ku, N., Cha, J.H., Lee, K.Y., Kim, J., Kim, T.W., Ha, S., Lee, D., 2010. Development of a mobile welding robot for double-hull structures in shipbuilding. *J. Mar. Sci. Technol.* 15, 374–385, <http://dx.doi.org/10.1007/s00773-010-0099-5>.
- Lai, R., Lin, W., Wu, Y., 2018]. Review of research on the key technologies, application fields and development trends of intelligent robots. In: Chen, Z., Mendes, A., Yan, Y., Chen, S. (Eds.), *Intelligent Robotics and Applications*. Springer, pp. 449–458, <http://dx.doi.org/10.1007/978-3-319-97589-4>.
- Laser sensor, (n.d.). <https://www.keyence.com.cn/products/sensor/laser/>. Accessed: 2020-04-29.
- Le, J., Zhang, H., Chen, X.Q., 2018. Realization of rectangular fillet weld tracking based on rotating arc sensors and analysis of experimental results in gas metal arc welding. *Robot. Comput. Manuf.* 49, 263–276, <http://dx.doi.org/10.1016/j.rcim.2017.06.004>.
- Lee, D., 2014. Robots in the shipbuilding industry. *Robot. Comput. Manuf.* 30, 442–450, <http://dx.doi.org/10.1016/j.rcim.2014.02.002>.
- Lei, T., Rong, Y., Xu, J., Huang, Y., 2018. Experiment study and regression analysis of molten pool in laser welding. *Opt. Laser Technol.* 108, 534–541, <http://dx.doi.org/10.1016/j.optlastec.2018.07.053>.
- Lei, T., Huang, Y., Shao, W., Liu, W., Rong, Y., 2020a. A tactful weld seam tracking method in super narrow gap of thick plates. *Robot. Comput. Manuf.* 62, 101864, <http://dx.doi.org/10.1016/j.rcim.2019.101864>.
- Lei, T., Wang, W., Rong, Y., Xiong, P., Huang, Y., 2020b. Cross-lines laser aided machine vision in tube-to-tubesheet welding for welding height control. *Opt. Laser Technol.* 121, 105796, <http://dx.doi.org/10.1016/j.optlastec.2019.105796>.
- Li, J., Zhao, H., Jiang, T., Zhou, X., 2008. Development of a 3D high-precise positioning system based on a planar target and two CCD cameras. *Int. Conf. Intell. Robot. Appl.* 475–484, http://dx.doi.org/10.1007/978-3-540-88518-4_51.
- Li, Y., Wang, Q., Fan, Z., Chen, H., Sun, Y., 2010. *Aperture detection and alignment control based on structured light vision*. Proc. 29th Chinese Control Conf. CCC'10, 3773–3778.
- Li, W., Ji, Y., Wu, J., Wang, J., 2015a. A modified welding image feature extraction algorithm for rotating arc narrow gap MAG welding. *Ind. Robot An Int.* 42, 222–227, <http://dx.doi.org/10.1108/IR-11-2014-0407>.
- Li, J., Yang, P., Huang, L., Xiao, M., 2015b. Recognition of initial welding position for large diameter pipeline based on pulse coupled neural network. *Ind. Robot. Int. J.* 42, 339–346, <http://dx.doi.org/10.1108/IR-01-2015-0011>.
- Li, X., Li, X., Khyam, M.O., Ge, S.S., 2017. Robust welding seam tracking and recognition. *IEEE Sens. J.* 17, 5609–5617, <http://dx.doi.org/10.1109/JSEN.2017.2730280>.
- Li, C., Shi, Y., Gu, Y.F., Yuan, P., 2018. Monitoring weld pool oscillation using reflected laser pattern in gas tungsten arc welding. *J. Mater. Process. Technol.* 255, 876–885, <http://dx.doi.org/10.1016/j.jmatprotec.2018.01.037>.
- Li, X., Liu, J., Wang, L., Wang, K., Li, Y., 2019. Welding process tracking control based on multiple model iterative learning control. *Math. Probl. Eng.* 2019, <http://dx.doi.org/10.1155/2019/6137352>.
- Li, J., Xu, X., 2018]. Research on tube-plate welding robot based on binocular vision. In: 2018 International Symposium on Sensing and Instrumentation in IoT Era, IEEE, <http://dx.doi.org/10.1109/ISSI.2018.8538078>.
- Liu, X., Wang, G., Shi, Y., 2006. Image processing of welding seam based on single-stripe laser vision system. *Proc. - ISDA 2006 Sixth Int. Conf. Intell. Syst. Des. Appl.*, 463–470, <http://dx.doi.org/10.1109/ISDA.2006.253881>.
- Liu, S., Wang, G., Shi, Y., 2008. *Simultaneous calibration of camera and hand-eye in robot welding with laser vision*. *J. South China Univ. Technol. Nat. Sci. Ed.* 36, 74–77.
- Liu, Z., Bu, W., Tan, J., 2010. Motion navigation for arc welding robots based on feature mapping in a simulation environment. *Robot. Comput. Manuf.* 26, 137–144, <http://dx.doi.org/10.1016/j.rcim.2009.09.002>.

- Liu, J., Zhu, S., Mao, F., Le, S., 2014. PID control of seam tracking based on particle swarm algorithm. *Hot Work. Technol.* 43, 159–161, <http://dx.doi.org/10.14158/j.cnki.1001-3814.2014.11.068>.
- Lü, X., Zhang, K., Wu, Y., 2017. The seam position detection and tracking for the mobile welding robot. *Int. J. Adv. Manuf. Technol.* 88, 2201–2210, <http://dx.doi.org/10.1007/s00170-016-8922-8>.
- Lü, X., Gu, D., Wang, Y., Qu, Y., Qin, C., Huang, F., 2018. Feature extraction of welding seam image based on laser vision. *IEEE Sens. J.* 18, 4715–4724, <http://dx.doi.org/10.1109/JSEN.2018.2824660>.
- Lv, N., Zhong, J., Chen, H., Lin, T., Chen, S., 2014. Real-time control of welding penetration during robotic GTAW dynamical process by audio sensing of arc length. *Int. J. Adv. Manuf. Technol.* 74, 235–249, <http://dx.doi.org/10.1007/s00170-014-5875-7>.
- Ma, H., Wei, S., Sheng, Z., Lin, T., Chen, S., 2010. Robot welding seam tracking method based on passive vision for thin plate closed-gap butt welding. *Int. J. Adv. Manuf. Technol.* 48, 945–953, <http://dx.doi.org/10.1007/s00170-009-2349-4>.
- Ma, X., Zhang, Y., 2011. Gas metal arc weld pool surface imaging: modeling and processing. *Weld. J. 90*.
- Micallef, K., Fang, G., Dinham, M., 2011]. Automatic seam detection and path planning in robotic welding. Lecture Notes in Electrical Engineering LNEE 88, 23–32, http://dx.doi.org/10.1007/978-3-642-19959-2_3.
- Mineo, C., Pierce, S.G., Nicholson, P.I., Cooper, I., 2016. Robotic path planning for non-destructive testing - A custom MATLAB toolbox approach. *Robot. Comput. Manuf.* 37, 1–12, <http://dx.doi.org/10.1016/j.rcim.2015.05.003>.
- Muhammad, J., Altun, H., Abo-Serie, E., 2018. A robust butt welding seam finding technique for intelligent robotic welding system using active laser vision. *Int. J. Adv. Manuf. Technol.* 94, 13–29, <http://dx.doi.org/10.1007/s00170-016-9481-8>.
- Nele, L., Sarno, E., Keshari, A., 2013. An image acquisition system for real-time seam tracking. *Int. J. Adv. Manuf. Technol.* 69, 2099–2110, <http://dx.doi.org/10.1007/s00170-013-5167-7>.
- Pablo, R.G., Manuel, R.M., 2019. Weld bead detection based on 3D geometric features and machine learning approaches. *IEEE Access* 7, 14714–14727, <http://dx.doi.org/10.1109/ACCESS.2019.2891367>.
- Peng, H., Zou, X., Xiong, J., Wu, D., Shen, J., She, Z., 2012. *Picking robot camera calibration system based on OpenCV. Adv. Mater. Res.* 430–432, 1963–1966, doi:10.4028/www.scientific.net/AMR.430-432.1963.
- Pinto-Lopera, J.E., Motta, J.M.S.T., Alfaro, S.C.A., 2016. Real-time measurement of width and height of weld beads in GMAW processes. *Sensors (Switzerland)*. 16, 1–14, <http://dx.doi.org/10.3390/s16091500>.
- Qi, Y., Jing, F., Tan, M., 2013. Line-feature-based calibration method of structured light plane parameters for robot hand-eye system. *Opt. Eng.* 52, 037202, <http://dx.doi.org/10.1117/1.oe.52.3.037202>.
- Reichert, C., Peterson, W., 2007. *Inspecting RSW electrodes and welds with laser-based imaging. Weld. J.* 86, 38–45.
- Robotic welding issues and challenges, (n.d.). <https://www.thefabricator.com/thefabricator/article/automationrobotics/robotic-welding-issues-and-challenges>. Accessed:2020-04-29.
- Rout, A., Deepak, B.B.V.L., Biswal, B.B., 2019. Advances in weld seam tracking techniques for robotic welding : a review. *Robot. Comput. Manuf.* 56, 12–37, <http://dx.doi.org/10.1016/j.rcim.2018.08.003>.
- Ryberg, A., Ericsson, M., Christiansson, A.K., Eriksson, K., Nilsson, J., Larsson, M., 2010. Stereo vision for path correction in off-line programmed robot welding. *Proc. IEEE Int. Conf. Ind. Technol.*, 1700–1705, <http://dx.doi.org/10.1109/ICIT.2010.5472442>.
- Saeed, G., Lou, M., Zhang, Y.M., 2004. Computation of 3D weld pool surface from the slope field and point tracking of laser beams. *Meas. Sci. Technol.* 15, 389–403, <http://dx.doi.org/10.1088/0957-0233/15/2/012>.
- Saeed, G., Zhang, Y.M., 2007. Weld pool surface depth measurement using a calibrated camera and structured light. *Meas. Sci. Technol.* 18, 2570–2578, <http://dx.doi.org/10.1088/0957-0233/18/8/033>.
- Schmidt, B., Wang, L., 2014. Automatic work objects calibration via a global-local camera system. *Robot. Comput. Manuf.* 30, 678–683, <http://dx.doi.org/10.1016/j.rcim.2013.11.004>.
- Shah, S., Aggarwal, J.K., 1996. Intrinsic parameter calibration procedure for a (high-distortion) fish-eye lens camera with distortion model and accuracy estimation. *Pattern Recognit.* 29, 1775–1788, [http://dx.doi.org/10.1016/0031-3203\(96\)00038-6](http://dx.doi.org/10.1016/0031-3203(96)00038-6).
- Shah, H.N.M., Sulaiman, M., Shukor, A.Z., 2017. Autonomous detection and identification of weld seam path shape position. *Int. J. Adv. Manuf. Technol.* 92, 3739–3747, <http://dx.doi.org/10.1007/s00170-017-0380-4>.
- Shao, W.J., Huang, Y., Zhang, Y., 2018. A novel weld seam detection method for space weld seam of narrow butt joint in laser welding. *Opt. Laser Technol.* 99, 39–51, <http://dx.doi.org/10.1016/j.optlastec.2017.09.037>.
- Sharifzadeh, S., Biro, I., Kinnell, P., 2020. Robust hand-eye calibration of 2D laser sensors using a single-plane calibration artefact. *Robot. Comput. Manuf.* 61, 101823, <http://dx.doi.org/10.1016/j.rcim.2019.101823>.
- Shen, H., Lin, T., Chen, S., Li, L., 2010. Real-time seam tracking technology of welding robot with visual sensing. *J. Intell. Robot. Syst. Theory Appl.* 59, 283–298, <http://dx.doi.org/10.1007/s10846-010-9403-1>.
- Shiu, Y.C., Ahmad, S., 1989. Calibration of wrist-mounted robotic sensors by solving homogeneous transform equations of the form $AX = XB$. *IEEE Trans. Robot. Autom.* 5, 16–29, <http://dx.doi.org/10.1109/70.88014>.
- Song, H., Zhang, Y., 2007. *Image processing for measurement of three-dimensional GTA weld pool surface. Weld. J.*
- Song, H., Zhang, Y.M., 2009. Error analysis of a three-dimensional GTA weld pool surface measurement system. *Weld. J. 88*.
- Stansfield, S.A., 1988. System utilizing passive vision and active touch. *Int. J. Rob. Res.* 7, 138–161.
- Sung, K., Lee, H., Choi, Y.S., Rhee, S., 2009. Development of a multiline laser vision sensor for joint tracking in welding. *Weld. J. (Miami, Fla.)*. 88.
- Tomei, P., 1991. Adaptive PD control for robot manipulators. *IEEE Trans. Robot.* 7, 565–570.
- Tsai, M.J., Lee, H.W., Ann, N.J., 2011. Machine vision based path planning for a robotic golf club head welding system. *Robot. Comput. Manuf.* 27, 843–849, <http://dx.doi.org/10.1016/j.rcim.2011.01.005>.
- Wang, Q., Jiao, W., Yu, R., Johnson, M.T., Zhang, Y.M., 2020. Virtual reality robot-assisted welding based on human intention recognition. *IEEE Transactions on Automation Science and Engineering* 17 (2), 799–808, <http://dx.doi.org/10.1109/TASE.2019.2945607>.
- Wei, S., Ma, H., Lin, T., Chen, S., 2010. Autonomous guidance of initial welding position with “single camera and double positions” method. *Sens. Rev.* 30, 62–68, <http://dx.doi.org/10.1108/026022810101010808>.
- Wei, S., Kong, M., Lin, T., Chen, S., 2011. Three-dimensional weld seam tracking for robotic welding by composite sensing technology. *Ind. Rob.* 38, 500–508, <http://dx.doi.org/10.1108/01439911111154072>.
- What is camera calibration?, (n.d.). <https://www.mathworks.com/help/vision/ug-camera-calibration.html>.Accessed:2020-04-29.
- Wu, Q.Q., Lee, J.P., Park, M.H., Jin, B.J., Kim, D.H., Park, C.K., Kim, I.S., 2015. A study on the modified Hough algorithm for image processing in weld seam tracking. *J. Mech. Sci. Technol.* 29, 4859–4865, <http://dx.doi.org/10.1007/s12206-015-1033-x>.
- Xiao, R., Xu, Y., Hou, Z., Chen, C., Chen, S., 2019. An adaptive feature extraction algorithm for multiple typical seam tracking based on vision sensor in robotic arc welding. *Sensors Actuators, A Phys.* 297, 111533, <http://dx.doi.org/10.1016/j.sna.2019.111533>.
- Xiong, J., Zhang, G., Qiu, Z., Li, Y., 2013. Vision-sensing and bead width control of a single-bead multi-layer part: material and energy savings in GMAW-based rapid manufacturing. *J. Clean. Prod.* 41, 82–88, <http://dx.doi.org/10.1016/j.jclepro.2012.10.009>.
- Xiong, J., Pi, Y., Chen, H., 2019. Deposition height detection and feature point extraction in robotic GTA-based additive manufacturing using passive vision sensing. *Robot. Comput. Manuf.* 59, 326–334, <http://dx.doi.org/10.1016/j.rcim.2019.05.006>.
- Xiong, J., Zhang, G., 2013. Online measurement of bead geometry in GMAW-based additive manufacturing using passive vision. *Meas. Sci. Technol.* 24, <http://dx.doi.org/10.1088/0957-0233/24/11/115103>.
- Xu, P., Tang, X., Lu, F., Yao, S., 2007a. An active vision sensing method for welded seams location using “circle-depth relation” algorithm. *Int. J. Adv. Manuf. Technol.* 32, 918–926, <http://dx.doi.org/10.1007/s00170-006-0410-0>.
- Xu, P., Tang, X., Na, R., Yao, S., 2007b. Study on welded seam recognition using circular laser vision sensor. *Chin. Opt. Lett.* 5, 328–331.
- Xu, P., Tang, X., Yao, S., 2008a. Application of circular laser vision sensor (CLVS) on welded seam tracking. *J. Mater. Process. Technol.* 205, 404–410, <http://dx.doi.org/10.1016/j.jmatprotoc.2007.11.268>.
- Xu, P., Xu, G., Tang, X., Yao, S., 2008b. A visual seam tracking system for robotic arc welding. *Int. J. Adv. Manuf. Technol.* 37, 70–75, <http://dx.doi.org/10.1007/s00170-007-0939-6>.
- Xu, Y., Yu, H., Zhong, J., Lin, T., Chen, S., 2012. Real-time seam tracking control technology during welding robot GTAW process based on passive vision sensor. *J. Mater. Process. Technol.* 212, 1654–1662, <http://dx.doi.org/10.1016/j.jmatprotoc.2012.03.007>.
- Xu, Y., Fang, G., Lv, N., Chen, S., Jia Zou, J., 2015. Computer vision technology for seam tracking in robotic GTAW and GMAW. *Robot. Comput. Manuf.* 32, 25–36, <http://dx.doi.org/10.1016/j.rcim.2014.09.002>.
- Xu, Y., Lv, N., Fang, G., Du, S., Zhao, W., Ye, Z., Chen, S., 2017. Welding seam tracking in robotic gas metal arc welding. *J. Mater. Process. Technol.* 248, 18–30, <http://dx.doi.org/10.1016/j.jmatprotoc.2017.04.025>.
- Xue, B., Chang, B., Peng, G., Gao, Y., Tian, Z., Du, D., Wang, G., 2019. A vision based detection method for narrow butt joints and a robotic seam tracking system. *Sensors (Switzerland)* 19, <http://dx.doi.org/10.3390/s19051144>.
- Yaskawa Motoman: Teaching Technology for Welding Robots, (n.d.). <https://www.automationworld.com/factory/robotics/product/13310598/yaskawa-motoman-teaching-technology-for-welding-robots>.Accessed:2020-04-29.
- You, D.Y., Gao, X.D., Katayama, S., 2014. Review of laser welding monitoring. *Sci. Technol. Weld. Join.* 19, 181–201, <http://dx.doi.org/10.1179/1362171813Y.0000000180>.
- Zeng, J., Chang, B., Du, D., Peng, G., Chang, S., Hong, Y., Wang, L., Shan, J., 2017. A vision-aided 3D path teaching method before narrow butt joint welding. *Sensors (Switzerland)* 17, <http://dx.doi.org/10.3390/s17051099>.
- Zeng, J., Cao, G.Z., Li, W.B., Chen, B.C., 2019]. An algorithm of hand-eye calibration for arc welding robot. In: 2019 16th International Conference on Ubiquitous Robots (UR), IEEE, <http://dx.doi.org/10.1109/URAI.2019.8768578>.
- Zha, J., Li, H., 2015. Analysis of the principle of laser displacement sensor and its application. *Appl. Mech. Mater.* 734, 84–89, <http://dx.doi.org/10.4028/www.scientific.net/amm.734.84>.
- Zhang, Z., 2000a. A flexible new technique for camera calibration. *IEEE Trans. Pattern Anal. Mach. Intell.* 22, 1330–1334, <http://dx.doi.org/10.1109/34.888718>.
- Zhang, Z., 2000b. A flexible new technique for camera calibration. *IEEE Trans. Pattern Anal. Mach. Intell.* 22, 1330–1334, <http://dx.doi.org/10.1109/34.888718>.
- Zhang, S., Huang, P.S., 2006. Novel method for structured light system calibration. *Opt. Eng.* 45, 083601, <http://dx.doi.org/10.1117/1.2336196>.

- Zhang, Y., Yang, X., 2012. A calibration method of binocular vision in laser remanufacturing robot. *Appl. Mech. Mater.* 101–102, 804–807, doi:10.4028/www.scientific.net/AMM.101-102.804.
- Zhang, W., Wang, X., Zhang, Y., 2013. Analytical real-time measurement of a three-dimensional weld pool surface. *Meas. Sci. Technol.* 24, <http://dx.doi.org/10.1088/0957-0233/24/11/115011>.
- Zhang, L., Ye, Q., Yang, W., Jiao, J., 2014a. Weld line detection and tracking via spatial-temporal cascaded Hidden Markov models and cross structured light. *IEEE Trans. Instrum. Meas.* 63, 742–753, <http://dx.doi.org/10.1109/TIM.2013.2283139>.
- Zhang, L., Ke, W., Ye, Q., Jiao, J., 2014b. A novel laser vision sensor for weld line detection on wall-climbing robot. *Opt. Laser Technol.* 60, 69–79, <http://dx.doi.org/10.1016/j.optlastec.2014.01.003>.
- Zhang, Z., Gao, H., Han, Q., Huang, R., Rong, J., Wang, Y., 2015a. Hand-eye calibration in robot welding of Aero tube. *J. Shanghai Jiaotong Univ.* 49 (392–394), 401.
- Zhang, Z., Chen, H., Xu, Y., Zhong, J., Lv, N., Chen, S., 2015b. Multisensor-based real-time quality monitoring by means of feature extraction, selection and modeling for Al alloy in arc welding. *Mech. Syst. Signal Process.* 60, 151–165, <http://dx.doi.org/10.1016/j.ymssp.2014.12.021>.
- Zhang, C., Li, H., Jin, Z., Gao, H., 2017. Seam sensing of multi-layer and multi-pass welding based on grid structured laser. *Int. J. Adv. Manuf. Technol.* 91, 1103–1110, <http://dx.doi.org/10.1007/s00170-016-9733-7>.
- Zhang, K., Chen, Y., Gui, H., Li, D., Li, Z., 2018a. Identification of the deviation of seam tracking and weld cross type for the derusting of ship hulls using a wall-climbing robot based on three-line laser structural light. *J. Manuf. Process.* 35, 295–306, <http://dx.doi.org/10.1016/j.jmapro.2018.08.014>.
- Zhang, L.Z., Xu, Y.L., Du, S.F., Zhao, W.J., Hou, Z., Chen, S.B., 2018b]. Point cloud based three-dimensional reconstruction and identification of initial welding position. In: *Transactions on Intelligent Welding Manufacturing*. Spring, pp. 61–77, http://dx.doi.org/10.1007/978-981-10-8330-3_4.
- Zhang, K., Yan, M., Huang, T., Zheng, J., Li, Z., 2019. 3D reconstruction of complex spatial weld seam for autonomous welding by laser structured light scanning. *J. Manuf. Process.* 39, 200–207, <http://dx.doi.org/10.1016/j.jmapro.2019.02.010>.
- Zhao, Y.M., Lin, Y., Xi, F., Guo, S., 2015. Calibration-based iterative learning control for path tracking of industrial robots. *IEEE Trans. Ind. Electron.* 62, 2921–2929, <http://dx.doi.org/10.1109/TIE.2014.2364800>.
- Zhu, Z.Y., Lin, T., Piao, Y.J., Chen, S.B., 2005. Recognition of the initial position of weld based on the image pattern match technology for welding robot. *Int. J. Adv. Manuf. Technol.* 26, 784–788, <http://dx.doi.org/10.1007/s00170-003-2053-8>.
- Zhu, J., Wang, J., Su, N., Xu, G., Yang, M., 2017. An infrared visual sensing detection approach for swing arc narrow gap weld deviation. *J. Mater. Process. Technol.* 243, 258–268, <http://dx.doi.org/10.1016/j.jmatprotec.2016.12.029>.
- Zou, Y., Chen, X., 2018. Hand-eye calibration of arc welding robot and laser vision sensor through semidefinite programming. *Ind. Rob.* 45, 597–610, <http://dx.doi.org/10.1108/IR-02-2018-0034>.
- Zou, Y., Wang, Y., Zhou, W., Chen, X., 2018a. Real-time seam tracking control system based on line laser visions. *Opt. Laser Technol.* 103, 182–192, <http://dx.doi.org/10.1016/j.optlastec.2018.01.010>.
- Zou, Y., Chen, X., Gong, G., Li, J., 2018b. A seam tracking system based on a laser vision sensor. *Measurement* 127, 489–500, <http://dx.doi.org/10.1016/j.measurement.2018.06.020>.



Youmin Rong received his Master's and Doctor's degrees from Huazhong University of Science and Technology in 2013 and 2017. He finished his postdoctoral research in 2019. Now he has worked at the school of mechanical science and engineering, Huazhong University of Science and Technology. He is the author or co-author of over 20 technical papers in the field of welding. He was the invited reviewer of multiple international journals. His research interests include welding monitor, numerical analysis, etc.



Hui Wang is a PhD candidate at the school of mechanical science and engineering, Huazhong University of Science and Technology from 2018. His research interests include automatic guided vehicle, SLAM, etc.



Yu Huang received his Doctor's degree from Huazhong University of Science and Technology in 2004. He is the Associate Director of State Key Lab of Digital Manufacturing Equipment and Technology and a Professor at Huazhong University of Science and Technology. He is a member of industrial automation committee of China mechanical engineering association. He has won 3 national scientific and technological process awards, including a First Prize, two Second Prize. His research interests include automatic guided vehicle, welding robot and intelligent manufacturing, etc.



Min Li received her Master's degree from Huazhong University of Science and Technology in 2006. Now She works as an associate professor at Key Lab of Optoelectronic Chemical Materials and Devices (Jianghan University), Ministry of Education. Her research interests include welding automation, digital manufacturing, etc.



Ting Lei is a PhD candidate at the school of mechanical science and engineering, Huazhong University of Science and Technology from 2017. He received his Bachelor of engineering and Master of engineering degrees from Changchun Institute of Technology in 2010 and Huazhong University of Science and Technology in 2013. He once worked as an assistant at Wuhan Donghu University from 2013 to 2017. He is a member of Hubei society of mechanical and electrical engineering. His research interests include machine vision, vision-aided robotic welding and weld seam tracking, etc.